e. Two specific publications/research papers of the applicant relevent to the research work mentioned above (Max: 2.5 MB)

The award is claimed based on the following two research publications which described ESAT-6 as an important virulent factor of *Mycobacterium tuberculosis* that interacts with host Beta-2 microglobulin (β2M), thereby i) inhibiting the protective CD8 T cell function by inhibiting β2M-MHC-1 interaction and 2) upregulate intracellular iron uptake by affecting β2M-HFE interaction. Thus ESAT-6 acts in a pleiotropic manner suppressing multiple host defense responses by directly interacting with β2M. Based on these findings two repurposed drugs (Mirabegron [SM09] and Olsalazine [SM15] were identified that specifically mask the methionine residue of ESAT-6 which is vital for the interaction with Asp53 residue of human β2M and thereby prevents interaction of ESAT-6 protein with β2M. This helps β2M to interact with MHC class I (***Jha et al.[2019] Journal of Immunology 203:1918***) as well as with HFE molecules of macrophages (***Jha et al.[2020]Journal of Immunology 205:3095***) increasing class I antigen presentation and decrease of iron uptake helping the host to restrict *M. tuberculosis* infection burden. Dr. Mukhopadhyay's research work identified for the first time novel virulence mechanism of ESAT-6, its moonlighting effects on mycobacterial virulence and ESAT-6-β2M as novel drug target of *M. tuberculosis*. Also Dr Mukhopadhyay for the first time identified two potent FDA approved drugs (Mirabegron and Olsalazine) that target ESAT-6-β2M with promising therapeutic effect. This has important implication to boost host protective responses which is promising to make a long term contribution in preventing infection and disease in countries with high burdens of TB.

1. Jha V, Rao RN, Janardhan S, Raman R, Sastry GN, Sharma V, Rao JS, Kumar D and **Mukhopadhyay S***. (2019). Uncovering structural and molecular dynamics of ESAT-6:β2M interaction: Asp53 of human β2-microglobulin is critical for the ESAT-6:β2M complexation. ***Journal of Immunology*** 203: 1918-1929 (Impact factor – 5.4)

2. Jha V, Pal R, Kumar D and **Mukhopadhyay S***. ESAT-6 protein of *Mycobacterium tuberculosis* increases holotransferrin-mediated iron uptake in macrophages by downregulating surface hemochromatosis protein HFE (2020). ***Journal of Immunology*** 205: 3095-3106. (Impact factor – 5.4)

***Corresponding author**

The Journal of Immunology

Uncovering Structural and Molecular Dynamics of ESAT-6: β2M Interaction: Asp53 of Human β2-Microglobulin Is Critical for the ESAT-6: β2M Complexation

Vishwanath Jha, Nagender Rao Rameshwaram, Sridhara Janardhan, Rajeev Raman, G. Narahari Sastry, Vartika Sharma, Jasti Subba Rao, Dhiraj Kumar and Sangita Mukhopadhyay

J Immunol 2019; 203:1918-1929; Prepublished online 4 September 2019;
doi: 10.4049/jimmunol.1700525
http://www.jimmunol.org/content/203/7/1918

The Journal of Immunology is published twice each month by
The American Association of Immunologists, Inc.,
1451 Rockville Pike, Suite 650, Rockville, MD 20852

Print ISSN: 0022-1767 Online ISSN: 1550-6606.

Uncovering Structural and Molecular Dynamics of ESAT-6:β2M Interaction: Asp53 of Human β2-Microglobulin Is Critical for the ESAT-6:β2M Complexation

Vishwanath Jha,*,†,1 Nagender Rao Rameshwaram,*,1 Sridhara Janardhan,‡ Rajeev Raman,§ G. Narahari Sastry,‡ Vartika Sharma,¶ Jasti Subba Rao,‖ Dhiraj Kumar,¶ and Sangita Mukhopadhyay*

ESAT-6 is a small secreted protein of *Mycobacterium tuberculosis* involved in the ESAT-6 secretion system (ESX-1)–mediated virulence and pathogenesis. The protein interacts with β2M, causing downregulation of MHC class I Ag presentation, which could be one of the mechanisms by which it favors increased survival of the bacilli inside the host. In an earlier study, we have shown that the C-terminal region of ESAT-6 is crucial for its interaction with β2M. However, the interface of β2M involved in interaction with ESAT-6 and detailed physicochemical changes associated with ESAT-6:β2M complexation are not fully defined. In this study, using computational and site-directed mutagenesis studies, we demonstrate the presence of strong noncovalent hydrophobic interactions between ESAT-6 and β2M in addition to the vital hydrogen bonding between the aspartate residue (Asp53) of β2M and methionine (Met93) of ESAT-6. Docking-based high-throughput virtual screening followed by 16-point screening on microscale thermophoresis resulted in the identification of two potent inhibitors (SM09 and SM15) that mask the critical Met93 residue of ESAT-6 that is required for ESAT-6:β2M interaction and could rescue cell surface expression of β2M and HLA in human macrophages as well as MHC class I Ag presentation suppressed by ESAT-6 in peritoneal macrophages isolated from C57BL/6 mice. Both SM09 and SM15 significantly inhibited intracellular survival of *M. tuberculosis* in human macrophages. Further, we characterized the physicochemical properties involved in the ESAT-6:β2M complexation, which may help in understanding host–pathogen interactions. ***The Journal of Immunology*****, 2019, 203: 1918–1929.**

The region of difference 1 (RD1) of the *Mycobacterium tuberculosis* genome encodes nine open reading frames (Rv3871 to Rv3879c) and has been considered to be important in the pathogenesis of *M. tuberculosis* (1–3). The RD1 is deleted in the bacillus Calmette-Guérin vaccine strains of *M. bovis* but present in all virulent strains of *M. tuberculosis* (3, 4). The open reading frames from Rv3866-Rv3881c of the *M. tuberculosis* genome encompassing the RD1 region is the ESAT-6 secretion system and referred to as ESX-1, which harbors two important genes: *esxA*, encoding the 6-kDa early secreted antigenic target (ESAT-6), and *esxB* encoding the 10-kDa culture filtrate protein 10 (CFP-10) (5, 6). ESAT-6 belongs to the WXG superfamily, in which the members are comprised of∼100 aa with a conserved Trp-X-Gly motif and Leu29 residue essential for biologically active conformation, secretion, and mycobacterial virulence (7–9). ESAT-6 deletion from the virulent strain of *M. bovis* resulted in attenuation of the bacilli in guinea pigs (10). In contrast, the reintroduction of RD1 into avirulent strains of *M. bovis* bacillus Calmette-Guérin reverted the phenotype back to full virulence (1).

ESAT-6 is shown to interact with CFP-10 in 1:1 tight complex and form helix-turn-helix structures that assemble antiparallel to each other (11, 12). It was revealed by two-dimensional electrophoresis that only the nonacetylated N-terminal region of ESAT-6 interacts with CFP-10 (13). A recombinant *M. tuberculosis* H37Rv strain (EsxAD84-95) expressing a mutant form of ESAT-6 with deletion of 12 aa from the C-terminal end had a functional ESX-1, but, compared with the strains expressing the wild-type ESAT-6, the mutant strain survived poorly in a mouse infection model (8, 12, 14). ESAT-6 protein is shown to modulate macrophage

*Laboratory of Molecular Cell Biology, Centre for DNA Fingerprinting and Diagnostics, Uppal, Hyderabad 500039, Telangana, India; †Graduate Studies, Manipal Academy of Higher Education, Manipal 576104, Karnataka, India; ‡Centre for Molecular Modeling, Council of Scientific and Industrial Research–Indian Institute of Chemical Technology, Tarnaka, Hyderabad 500007, Telangana, India; §Centre for Cellular and Molecular Biology, Council of Scientific and Industrial Research, Tarnaka, Hyderabad 500007, Telangana, India; ¶Cellular Immunology Group, International Centre for Genetic Engineering and Biotechnology, New Delhi 110067, India; and ‖Centre for Chemical Biology and Therapeutics, Institute for Stem Cell Science and Regenerative Medicine, Bangalore 560065, Karnataka, India

[1]V.J. and N.R.R. contributed equally to this work.

Received for publication April 20, 2017. Accepted for publication August 2, 2019.

This work was supported by grants from the Department of Biotechnology (DBT), Government of India (BT/PR12817/COE/34/23/2015), the Department of Science and Technology– Science & Engineering Research Board (DST–SERB), Government of India (EMR/2016/000644) and a core grant from the Centre for DNA Fingerprinting and Diagnostics by DBT (to the laboratory of S.M.). V.J. is supported by a fellowship from the Indian Council of Medical Research, Government of India. N.R.R. is supported by a DST–SERB grant (SB/YS/LS-135/2014).

Address correspondence and reprint requests to Dr. Sangita Mukhopadhyay, Laboratory of Molecular Cell Biology, Centre for DNA Fingerprinting and Diagnostics, Inner Ring Road, Uppal, Hyderabad 500039, Telangana, India. E-mail address: sangita@cdfd.org.in

The online version of this article contains supplemental material.

Abbreviations used in this article: ADME, absorption, distribution, metabolism, and excretion; ANS, 1-anilinonapthalene-8-sulphonate; CD, circular dichroism; CFP-10, culture filtrate protein 10; ER, endoplasmic reticulum; ESAT-6, 6-kDa early secreted antigenic target; ESX-1, ESAT-6 secretion system; ΔF_{norm}, change in the normalized fluorescence; β-gal, β-galactosidase; HFE, human hemochromatosis protein; HTVS, high-throughput virtual screening; ITC, isothermal titration calorimetry; MD, molecular dynamics; MST, microscale thermophoresis; QDO, quadruple drop out; RD1, region of difference 1; RMSD, root-mean-square deviation; RMSF, root-mean-square fluctuation; Trp, tryptophan.

immune responses and play an important role in *M. tuberculosis* virulence (15, 16).

In our previous study, we demonstrated that ESAT-6 protein alone or in complex with CFP-10 interacts with the host protein β-2-microglobulin (β2M). Deletion of the last 6 aa (VTGMFA) at the C-terminal end of ESAT-6 (ESAT-6ΔC) could prevent interaction of ESAT-6 with β2M, indicating that the C-terminal region (90–95 residues) of ESAT-6 protein is important for its interaction with β2M (17). β2M is an 11.6-kDa protein, adopting a β-sandwich Ig fold and is stable under physiological conditions. β2M is an L chain of MHC class I (18) and involved in MHC class I Ag presentation (19). We observed that ESAT-6 protein could downregulate the MHC class I Ag-presentation function of macrophage and $CD8^+$ T cell responses. ESAT-6 is shown to interact with and sequester β2M in the endoplasmic reticulum (ER) and thereby reduces the amount of β2M available for MHC class I–peptide complex formation (17). β2M is also noncovalently associated with several nonclassical MHC class I molecule–like human hemochromatosis proteins (HFE) (20) and an MHC class I–like molecule, CD1 (21). HFE is involved in iron metabolism (22), and CD1 molecules present glycolipid to CD1-restricted T cells (23). Thus, it is assumed that ESAT-6, by interacting with and sequestering β2M, could play an important role in modulating the host immune environment and offer favorable conditions for the advancement of infection (17). To gain some insights into the molecular mechanism of ESAT-6:β2M complexation and the biophysical parameters governing this interaction, in the current study, we have characterized the thermodynamic parameters and structural properties associated with ESAT-6 and β2M complex. Furthermore, the dynamics of the interaction at the interface of ESAT-6:β2M were studied, identifying the crucial residues of β2M that are engaged with ESAT-6 protein for complexation. Two small molecules (SM09 and SM15) that interact with ESAT-6 and rescued ESAT-6–mediated inhibition of MHC class I Ag presentation were also identified. Further, we showed that both SM09 and SM15 inhibited intracellular survival of *M. tuberculosis* inside macrophages. These molecules may further be exploited as novel drugs against *M. tuberculosis*

Materials and Methods

Purification of recombinant ESAT-6 and ESAT-6ΔC

ESAT-6 and ESAT-6ΔC were cloned in the pET-23a(+) vector with His-tag at the N-terminal region, and the recombinant protein was purified as previously described (17). Briefly, the ESAT-6 or ESAT-6ΔC clone was transformed into *Escherichia coli* BL21(DE3) cells, which were then grown in Terrific Broth containing 100 μg/ml ampicillin at 37°C until the OD reached 0.5 at 600 nm. The culture was induced with isopropyl thiogalactoside (IPTG), and the His-tagged ESAT-6 or ESAT-6ΔC protein was purified using Ni-NTA metal affinity resin (Clontech Laboratories) in denaturing conditions using 8 M urea (Sigma-Aldrich); the protein was refolded back to the native state by removal of urea in stepwise dilution as described earlier (17).

Isothermal titration calorimetry

Isothermal titration calorimetry (ITC) experiments were carried out with an iTC200 calorimeter (MicroCal) at 25°C. Recombinant ESAT-6 or ESAT-6ΔC and β2M (Sigma-Aldrich) proteins were extensively dialyzed in PBS (50 mM NaCl, 2.7 mM KCl, 10 mM Na_2HPO_4, 1.8 mM KH_2PO_4 [pH 7.4]), and the solutions were degassed before the experiment. ESAT-6 or ESAT-6ΔC at a 0.37 mM concentration was titrated to the sample cell filled with 0.012 mM β2M. During the experiment, the reaction mixture was continuously stirred at 1000 rpm by syringe. Typically, 1 μl injectant ESAT-6 or ESAT-6ΔC was added over 2 s with the spacing of 180 s between injections until the reaction reached saturation. Titration of ESAT-6 or ESAT-6ΔC to the buffer was also performed and subtracted for baseline correction. Heat change was recorded as differential power by the instrument, and thermodynamic parameters of interaction were determined by an integration of the obtained peak. Data on corrected heat changes were fitted using the nonlinear least square method to obtain parameters such as K_d, binding enthalpy (ΔH), and stoichiometry (n), using MicroCal ITC software (MicroCal).

Fluorescence spectroscopy

Fluorescence spectra of ESAT-6:β2M interaction was measured by using a Hitachi F-7000 spectrofluorometer (Hitachi). All spectra were recorded in correct spectrum mode with excitation and emission slits set at 5 nm. Intrinsic fluorescence of tryptophan (Trp) in protein was measured by exciting the solution at 295 nm, and emission spectra were recorded from 300 to 400 nm. Next, 5 μM β2M was titrated with increasing concentrations (0.25–5.2 μM) of ESAT-6 in PBS (pH 7.4). Protein solutions were mixed and incubated before recording the spectrum. Control experiments were measured by incubating different concentrations of ESAT-6 in the PBS and subtracted from spectra of the respective protein.

In 1-anilinonapthalene-8-sulphonate (ANS) fluorescence experiments, small aliquots of 10 mM ANS stock was added to the protein samples (ESAT-6, β2M, ESAT-6:β2M, ESAT-6ΔC, and ESAT-6ΔC:β2M complex; 5 μM each), and fluorescence spectra were recorded between 400 and 600 nm at an excitation wavelength of 365 nm. The final ANS concentration attained in each case was 100 μM. Fluorescence intensities were corrected for volume changes before further analysis of the ANS binding data.

Circular dichroism spectroscopy

Circular dichroism (CD) spectra were recorded on a JASCO J-815 Spectropolarimeter (JASCO) at room temperature. The path lengths used were 0.02 and 0.5 cm for far- and near-UV CD measurements, respectively. All spectra were recorded in PBS buffer with appropriate protein concentrations. The baseline spectra of buffer without protein were subtracted from the respective protein spectra. Effect on the β2M secondary structure was recorded by mixing increasing concentrations of ESAT-6 (1.25–20 μM) with 5 μM β2M followed by 6 h incubation at 4°C before recording. CD spectra of the ESAT-6:β2M complex was measured at an indicated temperature having a wavelength range of 190–250 nm. Near-UV spectra of ESAT-6, β2M, and the ESAT-6:β2M complex were measured in the wavelength range of 250–350 nm. Thermal stability of β2M, ESAT-6, ESAT-6:β2M, and ESAT-6ΔC:β2M complex (5 μM each) was monitored by measuring the ellipticity at a fixed wavelength (222 nm) as a function of temperature from 20 to 80°C with 1°C/min increment. The reversibility of protein unfolding was also examined by scanning the same sample and recording the CD spectra during cooling by a built-in temperature control unit. Further, the thermal melting point was deduced from unfolding experiments.

Generation of model systems using homology modeling and protein–protein docking

The structure of ESAT-6:CFP-10 complex downloaded from the Protein Databank (identification number 3FAV; A–D chains), consists of CFP-10 (A and C chains), ESAT-6 (B and D chains) proteins. The N-terminal region (MTEQQWNFA) and C-terminal region (AMASTEGNVTGMFA) amino acids of ESAT-6 were missing in the 3FAV structure. The sequence and structure of B chain ESAT-6 of 3FAV was used as a template and the complete sequence of ESAT-6 (Uniprot identification number P9WNK7) was considered as the target for building a homology model of ESAT-6 using Prime (version 3.5, 2014; Schrödinger). The assembled β2M-HLA-Nef complex (Protein DataBank identification 4U1M) containing a complex of β2M, HLA along with the HIV 1 of Nef protein was used as templates for β2M. Both ESAT-6 and β2M-HLA-Nef complex structures were prepared with respect to missing residues, fixing the formal charges, improper bond lengths, and overall geometry, followed by protein minimization using an OPLS2005 force field. The prepared structures were validated using the Ramachandran plot. For protein–protein docking and subsequent molecular dynamics (MD) simulations, the validated ESAT-6 and β2M-HLA-Nef complex structures were categorized into seven model systems: native ESAT-6 (system 1), ESAT-6ΔC (6 aa deleted from C-terminal region of ESAT-6) (system 2), ESAT-6 with β2M (system 3), ESAT-6 with β2M (mutation of Asp53Ala in β2M; designated also as Asp73 in β2M with signal sequence) (system 4), ESAT-6ΔC with β2M protein (system 5), β2M-HLA-Nef complex (system 6), and β2M (Asp53Ala)-HLA-Nef complex (system 7).ESAT-6 is known to sequester β2M in the ER, downregulating complex formation and surface expression of β2M along with the MHC class I family of proteins that are involved in Ag presentation and iron regulation. Thus, ESAT-6 is involved in undermining the host protective responses and favoring *M. tuberculosis* survival inside the host (17).

The C-terminal region of ESAT-6 has a prominent role in interaction with β2M, but the region of β2M that has crucial effects on complexation of ESAT-6:β2M is not known. To understand the binding mode and investigate the key active site of noncovalent residues of the ESAT-6:β2M interaction, a protein–protein docking study was performed using Bioluminate (version 3.5, 2014; Schrödinger). In protein–protein docking, no constraints were imposed, and standard mode was used with the default value of the number of ligand rotations to a probe of 70,000. A maximum of 50 poses were saved. The Piper algorithm samples all possible orientations of the two selected proteins. The docked protein complexes were analyzed for their noncovalent interactions. The selected pre-eminent poses were further subjected to MD simulations to decipher the protein conformational changes and their stability.

MD simulations

The seven model systems resulting from the protein–protein docking obtained in the foregoing section were subjected to MD simulations at 10 ns using the Desmond module of the Schrödinger suite. MD simulation studies followed five steps: simulation setup, relaxing the model system, running the simulation, viewing the trajectories, and analyzing the results. The simulation setup was performed with the simple point charge solvent model along with the orthorhombic box shape, having 10Å × 10Å × 10Å distances around the complex and further box volume was minimized. The total atoms in the model systems from one to seven consist of 18,908; 18,481; 30,283; 30,187; 30,451; 50,182; and 50,206 atoms, respectively. Each system was neutralized with counter ions with an NaCl concentration 0.15 M. The initial MD simulations were performed with OPLS2005 force field, and SHAKE algorithm was used along with periodic boundary conditions to restrain the geometry of water molecules and heavy atom bond lengths with hydrogens; electrostatic interactions were applied using the Particle Mesh Ewald method (24, 25). The model systems were simulated with NPT ensemble (constant number of atoms N, pressure P, and temperature T) for a 10-ns simulation time, pressure 1 bar, and temperature of 27°C. A time step of 2 fs was used for the equilibration stages. Trajectories after every 50 ps were recorded. The model systems were used to comprehend the role of each amino acid in terms of noncovalent interactions (Supplemental Table I), root-mean-square deviation (RMSD), and root-mean-square fluctuation (RMSF) throughout the MD simulations. MD simulations protocol was also used for ESAT-6:ligand complexes (SM09 and SM15) derived from molecular docking, in which system 1 (only ESAT-6) was used as a control.

Yeast two-hybrid interaction and site-directed mutagenesis

ESAT-6 was cloned in frame with the GAL binding domain of pGBKT7 construct using the forward primer (5′-GGAATTCCATATGATGACAGAGCAGCAGTGGAATTTCG-3′) and reverse primer (5′-CGCGGATCCCTATGCGAACATCCCAGTGACGTTG-3′). Full-length β2M was cloned in the GAL activating domain of pGADT7, using a forward primer (5′-ATATCATATGATGTCTCGCTCCGTGGCC-3′) and reverse primer (5′-ACGCGGATCCTTACATGTCTCGATCCCAC-3′), respectively. The β2M mutant (Asp53Ala) was generated by site-directed mutagenesis, using a specific set of primers and overlap extension PCR: set 1 (forward: 5′-ATATCATATGATGTCTCGCTCCGTGGCC-3′ and reverse: 5′-CTTGCTGAAAGACAAAGCTGAATGCTCCACTTT-3′); set 2 (forward: 5′-AAAGTGGAGCATTCAGCTTTGTCTTTCAGCAAG-3′ and reverse: 5′-ACGCGGATCCTTACATGTCTCGATCCCAC-3′). AH109 yeast strain was cotransformed with pGBKT7–ESAT-6 and pGADT7–native β2M or pGADT7–β2M (Asp53Ala) plasmid constructs. Transformed colonies were plated and grown on SD/–Ade/–His/–Leu/–Trp medium quadruple drop out (QDO plate) for 5 d at 30°C to examine expression of ADE2 and HIS3. The interaction between ESAT-6 and β2M was observed by checking the expression of the reporter gene (ADE2, HIS3, and LacZ) in the AH109 strain. The positive interactions of ESAT-6 and β2M or β2M (Asp53Ala) were determined by the growth of yeast colonies on the QDO plate or by measuring β-galactosidase (β-gal) expression using a colorimetry immunoassay (26), as described by the manufacturer (Roche). The pGBKT7–ESAT-6/pGADT7–native β2M and pGBKT7/pGADT7–native β2M were used as positive and negative controls, respectively.

Western blotting

Transformed yeast cells were grown in selective media (QDO) and harvested by centrifugation in sterile water. Pellets were resuspended in lysis buffer (50 mM Tris [pH 7.5], 150 mM NaCl, 1 mM PMSF, 1× protein inhibitor mixture [Roche]) and lysed using a bead beater (MP Biomedicals). The cell lysate was resolved in 16% Tris–Tricine SDS-PAGE and then transferred to nitrocellulose membranes. Further, the blots were probed with the appropriate combination of primary Ab and HRP-conjugated secondary Ab (Sigma-Aldrich). The bound HRP was detected by chemiluminescence following the manufacturer's protocol (GE Healthcare).

High-throughput virtual screening

Modeled ESAT-6 structure (system 1) was used for the active site grid generation for molecular docking-based high-throughput virtual screening (HTVS). A total of 2950 compounds with antimicrobial activity were collected from BioPhytMol (30), GlaxoSmithKline (177), ChEMBL (2371), and DrugBank (372) for docking-based HTVS using the Glide modules of Schrödinger. The docked compounds were prioritized according to the docking score and its key active site interactions. Further, prioritization of the compounds has been subjected to permeability prediction and the absorption, distribution, metabolism, and excretion ADME properties using the SwissADME tool (http://www.swissadme.ch/). Seventeen compounds were short listed, based on a high Glide docking score and ADME properties. These compounds were procured from commercial vendors (AK Scientific and AKos) and designated as SM01 to SM17 (Supplemental Table II).

Microscale thermophoresis

ESAT-6 used in the assay was labeled with NT-647-NHS fluorescent dye using the Monolith NT Protein Labeling Kit RED-NHS (NanoTemper Technologies). Assays were carried out in 20 mM Tris buffer (pH 7.4) with 200 mM NaCl, 0.05% Tween 20, and 2 mM DTT. For the direct binding assay, 10 μl of labeled ESAT-6 protein at a final concentration 20 nM was mixed with 10 μl of test compound (5 μM) (Supplemental Table II) and incubated on ice for 10 min. Direct binding was determined using a single point screening on microscale thermophoresis (MST). For the competitive assay, 10 μl of labeled ESAT-6 protein at a final concentration 15 nM was mixed with 600 nM β2M at the EC_{80} concentration determined by prior titration using a 16-point serial dilution by direct binding MST. For both the assays, samples prepared as above were centrifuged at 15,000 rpm at 4°C for 10 min, and 4 μl of the supernatant was loaded into Premium Coated Capillaries Monolith NT.115 (NanoTemper Technologies). MST analysis was performed at MST power of 40% and LED power of 80% at a temperature of 22°C using the red detection channel of a Monolith NT.115. An initial "Capillary Scan" was performed to scan for fluorescence across the length of the capillary tray to determine the exact position of each capillary before the MST measurement was started. Compounds displaying high amplitude were assayed at 16 different concentrations by serial dilution, and data were analyzed using NanoTemper analysis software. K_d values were determined using "T-jump plus Thermophoresis" settings. The change in thermophoresis between different experimental conditions was expressed as the change in the normalized fluorescence (ΔF_{norm}), which is defined as F_{hot}/F_{cold} (F-values corresponding to average fluorescence values between defined areas in the curve under steady-state conditions of control (F_{cold}) or experimental (F_{hot}) conditions. Titration of the nonfluorescent ligand causes a gradual change in thermophoresis, which is plotted as ΔF_{norm} to yield a binding curve, which was then fitted to derive binding constants (27).

Animals

C57BL/6 mice were maintained at the animal house facility of Vimta Labs Hyderabad, and the experimental protocols were approved by and performed as per the guidelines of the Institutional Animal Ethics Committee of Vimta Labs Hyderabad.

Cell culture

Human monocyte THP-1 cells were obtained from National Centre for Cell Science, Pune, India. THP-1 cells were cultured in complete RPMI 1640 containing 10% (v/v) heat-inactivated FBS (Hyclone) and 1× Glutamax (Thermo Fisher Scientific), 1× Antimycotic-Antibacterial (Life Technologies). Mice peritoneal macrophages were isolated as described earlier (17, 28). In brief, 6–8-wk-old C57BL/6 mice were injected with 1 ml of 4% thioglycolate i.p. After 4 d, mice were sacrificed, and peritoneal macrophages were harvested. Cells were cultured in complete DMEM containing 10% (v/v) FBS, 1× Glutamax, and 1× Antimycotic-Antibacterial.

MHC class I Ag presentation assay

The MHC class I Ag presentation assay was carried out in vitro using B3Z, a kind gift from Dr. Satyajit Rath and Dr. Vineeta Bal (National Institute of

Immunology, New Delhi, India), which is a $CD8^+$ T cell hybridoma specific for $OVA_{257–264}$ (SIINFEKL) presented on the murine H-$2K^b$ MHC class I molecule (29), and thioglycolate-elicited peritoneal macrophages from C57BL/6 mice (H-2^b) as APCs. Hypertonic loading of OVA into the cytoplasm followed by osmotic lysis of pinosomes containing OVA was used to load OVA peptides on MHC class I for presentation of soluble Ag via the MHC class I Ag presentation pathway, as described earlier (17, 30). In brief, macrophages were pretreated for 2 h at 37°C with 12.5 μM recombinant ESAT-6 protein in the absence or presence of equimolar SM09 or SM15 inhibitor. Next, the cells were washed with incomplete DMEM and incubated with hypertonic serum-free DMEM containing 0.5 M sucrose, 10% polyethylene glycol 1000, and 10 mg/ml OVA (Sigma-Aldrich) or BSA (Sigma-Aldrich) for 10 min at 37°C. Then hypotonic DMEM (60% DMEM and 40% water) was added for 2 min at 37°C followed by washing and further incubation for 2 h to allow OVA Ag processing and presentation by the MHC class I molecules. Next, OVA-loaded APCs (2×10^5) were fixed in 0.5% paraformaldehyde and cocultured with B3Z T cells (1×10^5) in a 96-well tissue culture plate for 24 h (31). The supernatants containing IL-2 secreted by the B3Z T cells were harvested, and IL-2 levels were measured by ELISA following the manufacturer's protocol (eBioscience).

Flow cytometry

THP-1 cells were differentiated into macrophages by incubating cells with 5 ng/ml PMA (Sigma-Aldrich) for 12 h, followed by a resting period of 24 h. Next, these macrophages were treated with 12.5 μM of ESAT-6 protein in the absence or presence of equimolar SM09 or SM15 inhibitor for 2 h in incomplete RPMI 1640. Cells were harvested and stained in FACS staining buffer (1% BSA in 1× PBS containing 0.01% sodium azide) containing either PE-conjugated anti-β2M Ab or FITC-conjugated anti-HLA Ab (BD Biosciences) for 1 h at 4°C. Surface expression of β2M or HLA was studied by flow cytometry (FACSAria; BD Biosciences). The cell population was gated on the basis of scattered plot in FlowJo software. The dead cell debris had a lower level of forward scatter, which was excluded and analyzed in FlowJo software with acquisition of 20,000 events per sample.

Infection of THP-1 macrophages

H37Rv *M. tuberculosis* bacteria were cultured in 7H9 Middlebrook (BD Difco) medium supplemented with 10% oleic albumin dextrose catalase (BD Difco) and 0.05% Tween 80 (Rolex Chemicals) until the log phase was attained. Single-cell suspension of the bacterial cultures was prepared by passing the cultures through a 23-, 26-, and 30-gauge syringe. PMA-differentiated THP-1 macrophages were infected with H37Rv *M. tuberculosis* at multiplicity of infection 1:10 in antibiotic-free complete medium for 4 h. The extracellular bacteria were killed by incubating the infected cells with amikacin sulfate (final concentration 200 μg/ml) for 2 h. Next, the medium was removed and fresh medium containing 12.5 μM small molecules (SM09, SM15) was added. The CFU count was performed after lysing the cells in 0.06% SDS at 12- and 24-h postinfection and plating the lysate in 7H11 agar supplemented with 10% OADC. Macrophages treated in medium alone or DMSO were used as controls.

Statistics

Data were expressed as mean ± SEM of three different experiments performed in a similar way. Individual data were analyzed using the Student *t* test. Calculations were performed using GraphPad Prism. For CFU counting, one-way ANOVA followed by the Bonferroni posttest was used, and a p value <0.05 was considered to be significant.

Results

ESAT-6:β2M interaction and binding energetics

ITC was performed to calculate the energetics of ESAT-6 interaction with β2M at 25°C. ESAT-6 binding to β2M was an endothermic reaction as depicted by the thermogram corresponding to a plot of integrated heats as a function of the molar ratio of ESAT-6:β2M (Fig. 1A). ESAT-6 binding to β2M was entropy driven, with the overall K_d of 6.9 μM. The binding isotherms indicated absorption of heat upon binding of ESAT-6 to β2M and the thermodynamic parameters best fit with one set of a site with a stoichiometry of interaction equals to one. The energetic values for binding isotherm of ESAT-6:β2M were as follows: change in enthalpy ($\Delta H = 36.6 \pm 8.7$ kcal/mol), change in entropy ($T\Delta S = 43.8$ kcal/mol) and free energy change ($\Delta G = -7.21$ kcal/mol) with a K_a ($K_a = 1.44 \times 10^5 \pm 1.61 \times 10^4\ M^{-1}$). These studies indicate that ESAT-6 binding is positively stabilized by an entropic factor. ESAT-6ΔC was used as a control

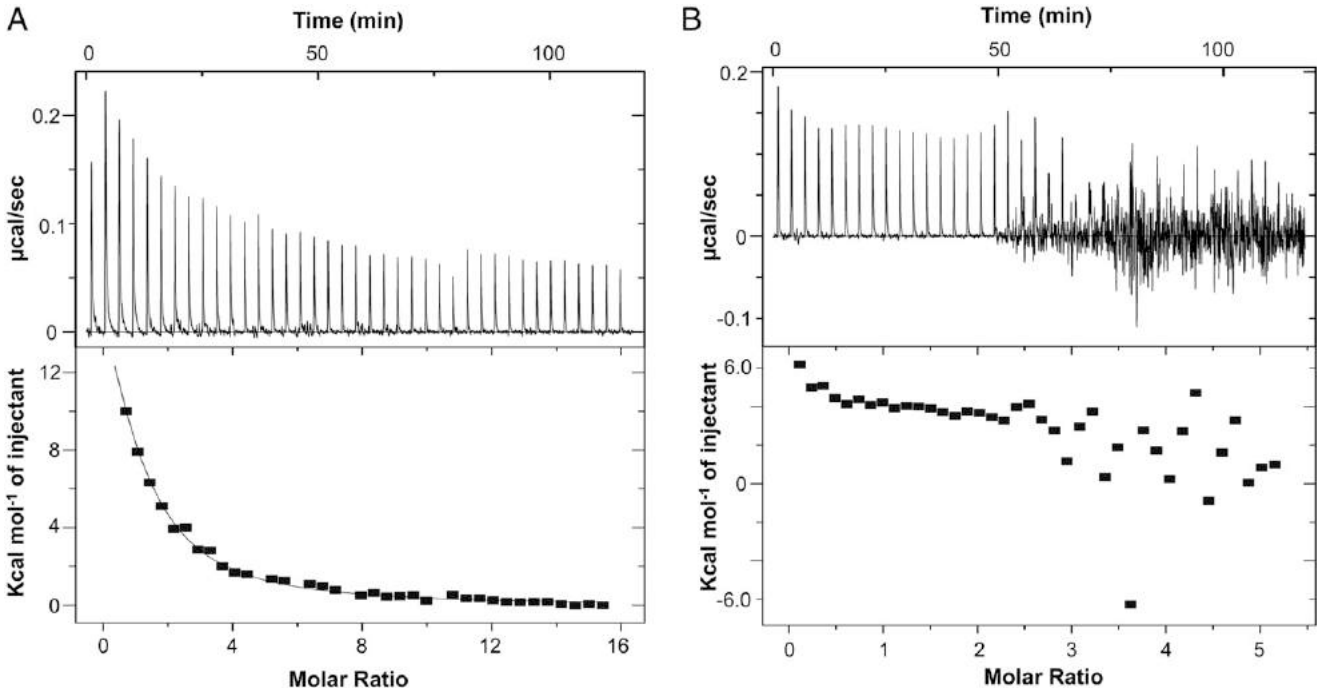

FIGURE 1. Thermodynamics of (**A**) ESAT-6:β2M, (**B**) ESAT-6ΔC:β2M interaction by ITC. A representative titration of ESAT-6 or ESAT-6ΔC with β2M in PBS at 25°C. A sample cell of ITC containing β2M was titrated against an increasing concentration of ESAT-6 or ESAT-6ΔC. The upper thermogram panel shows the observed heats for each injection of ESAT-6 at 180-s intervals after baseline correction, whereas the lower panel depicts the binding enthalpies versus protein molar ratio. The data (filled squares) are fitted to best-fitted site binding model. Data are representative of three different experiments.

that, as expected, did not show any interaction with β2M (17) (Fig. 1B).

The effect of hydrophobic interactions on the ESAT-6:β2M complex

ESAT-6:β2M complex is stable at a higher salt concentration, indicating that the nature of the interaction between ESAT-6 and β2M is probably stabilized by hydrophobic interaction. To confirm the role of hydrophobic interaction between ESAT-6 and β2M, an ANS binding assay was performed. The fluorescence spectra and binding curve corresponding to the ANS with ESAT-6, β2M, ESAT-6:β2M, ESAT-6ΔC, and ESAT-6ΔC:β2M complex are shown in Fig. 2. ANS binding with ESAT-6 leads to an increase in the fluorescence intensity of the ANS, and the magnitude of the change in fluorescence decreases with increasing ANS concentration. However, in the case of the ESAT-6:β2M complex, in which ESAT-6 is associated with β2M, fluorescence intensity decreases and λ_{max} red shifted to 538 nm compared with ESAT-6 alone (λ_{max} 521 nm) (Fig. 2A). This observation indicates that the solvent-exposed hydrophobic surface of ESAT-6 moves toward the less polar environment at the interface of interaction during complex formation. As expected, ESAT-6ΔC and ESAT-6ΔC:β2M showed similar fluorescence intensity because of the absence of interaction between ESAT-6ΔC and β2M (Fig. 2B).

Conformation change in β2M structure upon interaction with ESAT-6

To characterize conformational changes in β2M upon interaction with ESAT-6 protein, we determined intrinsic Trp fluorescence and transitions in the secondary structure using fluorescence and CD (near-UV and far-UV) spectroscopy. The fluorescence emission spectra of β2M showed a λ_{max} 339.8 nm; however, with increasing concentration of ESAT-6, the λ_{max} red shifted to 340.4 nm, accompanied by a decrease in fluorescence intensity (Fig. 3A). Further, conformational changes in the secondary structure of β2M upon binding with ESAT-6 were determined by the CD by recording spectra in far-UV and near-UV regions. In the far-UV region, native β2M displayed typical β-sheet conformation, as inferred by maxima at 201 nm and minima at 219 nm. However, increasing the concentration of ESAT-6 resulted in a shift of the positive peak below 201 nm, along with more positive ellipticity with respect to β2M and increase in negative ellipticity toward 190 nm. This suggests conformational changes in β2M during complex formation with ESAT-6 (Fig. 3B). Near-UV CD spectra of β2M showed a positive peak at 265 and 290 nm, consistent with the aromatic amino acids packing in specific conformation in native β2M protein (Fig. 3C). ESAT-6 did not show any significant tertiary structure in near-UV spectra. The complex formation (ESAT-6:β2M) resulted in a significant decrease in the intensity in near-UV spectra. This suggests that the tertiary structure of β2M changes relative to its native conformation upon binding with ESAT-6.

Thermal stability of the ESAT-6:β2M complex

To substantiate the stability of ESAT-6:β2M complex, it is important to study the stability of the ESAT-6, β2M, and ESAT-6:β2M complex more precisely and also to understand the nature of the unfolding transition. The change in the CD signal at 222 nm, corresponding to the positive maximum in the far-UV CD spectrum, was determined as a function of temperature. ESAT-6 exhibited an unfolding transition at 24˚C, whereas β2M which is stable, undergoes an unfolding transition at~60˚C (Fig. 4A, 4B). Thus, a temperature scan of ESAT-6:β2M (melting temperature = 64˚C) complex displayed a decrease in the ellipticity marginally between 20 and 60˚C but experienced a steep drop of ellipticity between 60 and 80˚C and remained low upon a further increase in temperature with respect to the individual proteins ESAT-6 and β2M (Fig. 4C). However, the unfolding transition of ESAT-6:β2M is increased by 4˚C (64˚C), suggesting that ESAT-6 in complex with β2M is stabilized in physiological condition. In contrast, because of the absence of interaction between ESAT-6ΔC and β2M, the ESAT-6ΔC:β2M complex displayed unfolding transition at ~60˚C, similar to β2M (Fig. 4D).

Molecular docking and MD simulations of ESAT-6:β2M complexation

All promising binding modes and key active site interactions of ESAT-6– and β2M-docked complexes obtained were carefully analyzed. The prioritized unrivaled docked poses that retain the C-terminal region of ESAT-6 residue interaction with the Asp53 residue of β2M were subjected to 10-ns MD simulations. For all the model systems obtained before and after MD simulations, we analyzed the RMSD, RMSF for all the trajectories with respect to simulation time, along with the noncovalent interactions such as hydrophobic (5 Å), main chain–side chain hydrogen bonds, side chain–side chain hydrogen bonds, sulfur–sulfur bridges, ionic (6 Å), aromatic–aromatic (4.5 to 7 Å), aromatic–sulfur (5.3 Å), and cation-π (6 Å). The detailed noncovalent interaction profile for all model systems is presented in Supplemental Table I.

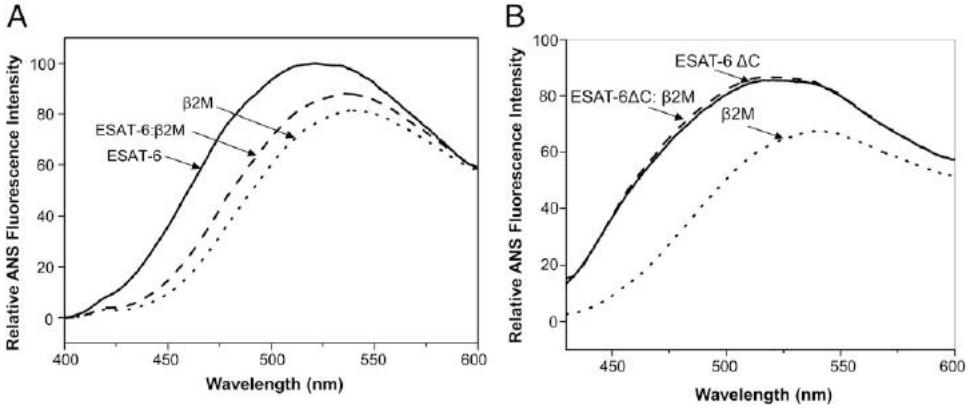

FIGURE 2. ANS binding assay. (**A**) Decrease in fluorescence intensity of ANS binding to ESAT-6 and red shift of λ_{max} 538 nm in ESAT-6:β2M complex indicates that the solvent-exposed hydrophobic surface of ESAT-6 is hindered in the presence of β2M. (**B**) The fluorescence spectra of ANS binding to ESAT-6ΔC, ESAT-6ΔC:β2M, and β2M. Because of absence of interaction between ESAT-6ΔC and β2M, there was no change in the ANS fluorescence of ESAT-6ΔC, ESAT-6ΔC:β2M. Data are representative of three different experiments.

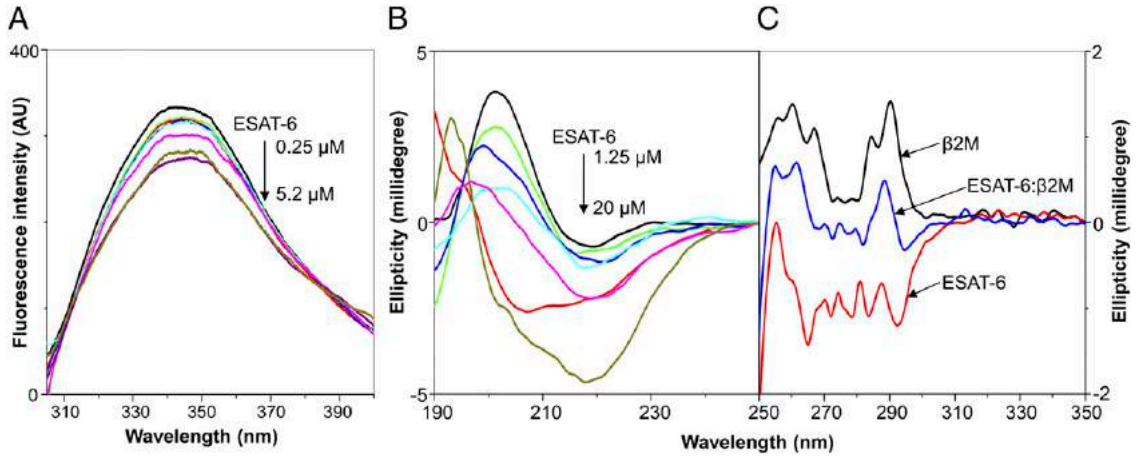

FIGURE 3. Conformational change of β2M structure upon binding with ESAT-6. (**A**) Steady-state fluorescence spectra of β2M titrated with various concentrations of ESAT-6. The arrow indicates a change in fluorescence intensity that takes place upon addition of an increasing concentration of ESAT-6. The spectra are normalized against titration of ESAT-6 only with buffer. (**B**) Far-UV CD spectra of β2M with different concentrations of ESAT-6. Decreased ellipticity was observed with the addition of ESAT-6. (**C**) Near-UV CD spectra of β2M, ESAT-6, and ESAT-6:β2M complex. Data are representative of three different experiments.

From our MD simulation analysis, we observed that the noncovalent hydrophobic interactions were more predominant as compared with the electrostatic interactions for obtaining strong binding affinity and thermal stability between ESAT-6 and β2M. We observed that among the seven aspartic acid residues of β2M (Asp34, Asp38, Asp53, Asp59, Asp76, Asp96, and Asp98), the Asp53 residue exhibited significant contribution in interaction with ESAT-6 (Fig. 5A, Supplemental Fig. 1A). MD simulations revealed that Asp53B:N (nitrogen atom of aspartic acid of chain B) exhibited main chain–side chain strong hydrogen bond interaction with Met93A:O (oxygen atom of methionine chain A) of ESAT-6 in model system 3 (Fig. 5A), whereas, in mutated model systems (4, 5), the hydrogen bond interactions were lost (Fig. 5B, Supplemental Table I). The Met93 residue of ESAT-6 maintained hydrogen bond interaction with the Asp53 residue of β2M from trajectory number 100 to 250, indicating the vital role of these residues in ESAT-6:β2M complexation (Fig. 5C). We also observed 5.65Å structural deviation (RMSD) for the last trajectory in backbone Cα of the system 4 in comparison with the system 3 (Fig. 5D). Additionally, the model system 3 exhibited Arg12B:NE-Asn89A:O side chain–side chain hydrogen bond interaction, Arg12B-Glu3A ionic interaction, Phe22B–Val90A, Tyr26B–Trp6A, Phe56B–Ile18A, Phe56B–Leu72A, Phe56B–Ile76A, Trp60B–Ile18A, Trp60B–Leu69A, Trp60B–Leu72A, Tyr63B–Trp6A, Tyr63B–Met93A, Leu65B–Met93A, Tyr67B–Val90A, and Tyr67B–Phe94A hydrophobic interactions and Tyr26B–Trp6A, Tyr67B–Phe94A, Tyr67B–Phe94A aromatic–aromatic interactions for the stability of the proteins; however, these noncovalent interactions were missing in systems 4 and 5. RMSD and RMSF plots for backbone Cα for model systems at 10 ns of MD simulations are shown in Supplemental Fig. 2. The results indicated that ESAT-6 and β2M possess strong hydrophobic interactions at the surface along with other noncovalent interactions, exemplifying the host–pathogen interactions at the molecular level.

Asp53 residue of β2M is important to form a complex with ESAT-6

Our previous studies have indicated that ESAT-6 interacts with β2M, and the C-terminal region of ESAT-6 is crucial for the interaction. We also observed that ESAT-6 interacts with the free form of β2M with or without a signal sequence (17). However, the region of β2M having a role in the interaction with ESAT-6 was not identified. To classify the regions involved in the ESAT-6:β2M complex, β2M was mapped to pin down the residues involved in the interaction. Results from our docking and MD simulation studies have indicated that the Asp53 residue in β2M has an important role in stabilization of the ESAT-6:β2M complex. To validate the significance of Asp53 residue and strength of interaction, a yeast two-hybrid assay was performed using the ESAT-6 cloned in the pGBKT7 vector (pGBKT7–ESAT-6) and native or Asp53 mutant β2M (Asp53Ala) cloned in pGADT7

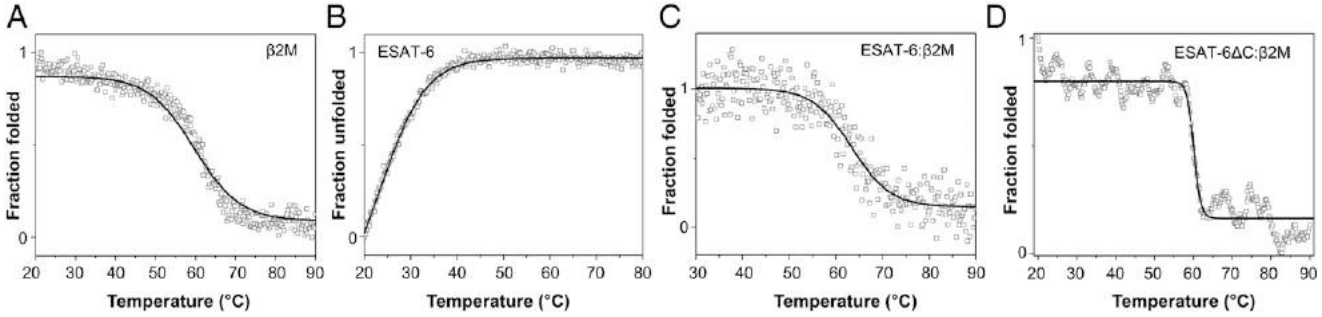

FIGURE 4. Thermal unfolding of (**A**) β2M, (**B**) ESAT-6, (**C**) ESAT-6:β2M complex, and (**D**) ESAT-6ΔC:β2M measured at (pH 7) with PBS and monitored by CD spectroscopy at 222 nm as a function of temperature. The temperature was increased from 20 to 90°C at 1°C/min, and ellipticity versus temperature was plotted. These thermal-unfolding studies illustrate that ESAT-6:β2M is more stable compared with the individual proteins ESAT-6 and β2M. Data are representative of three different experiments.

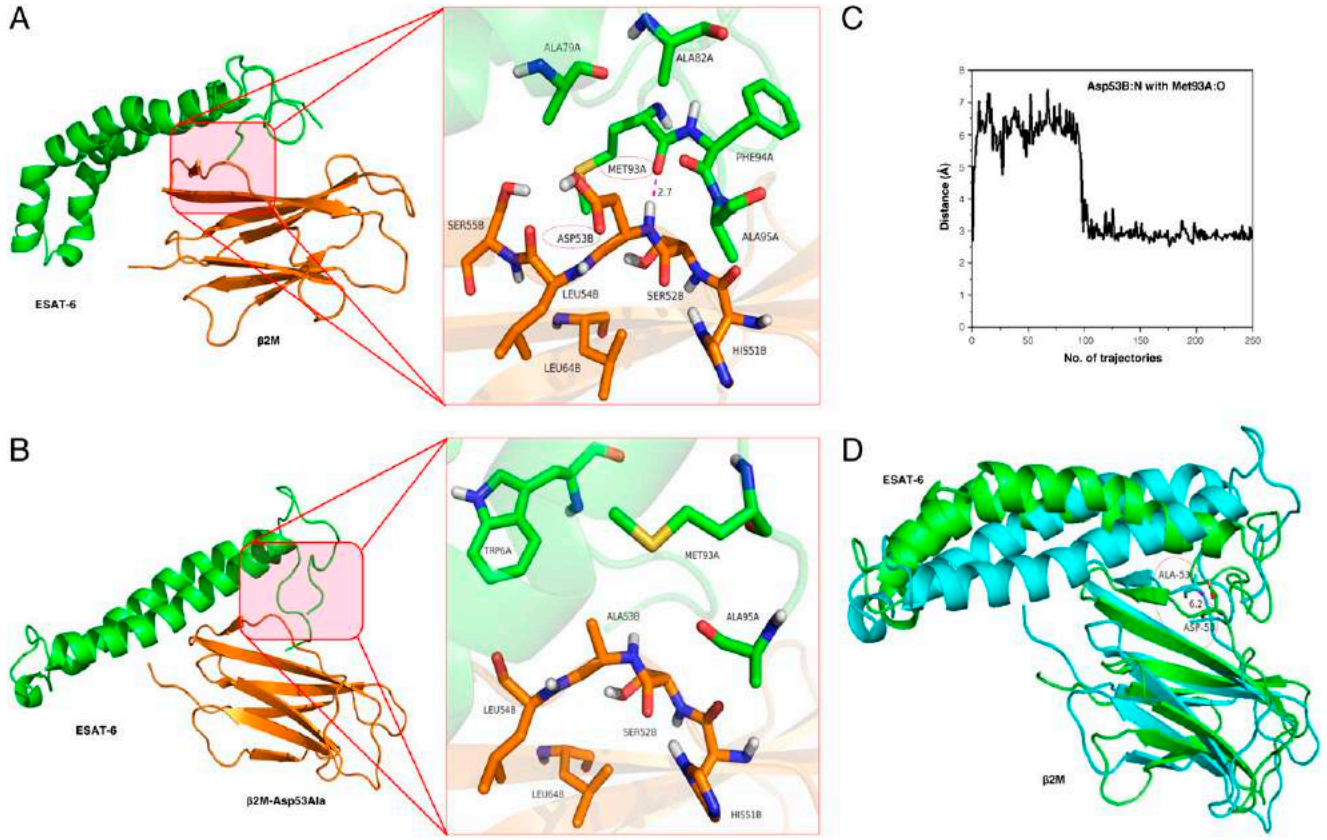

FIGURE 5. Key active site residues of the ESAT-6 protein and β2M protein interface. The complex structures were obtained from protein–protein docking followed by 10-ns MD simulations. (**A**) The interface of ESAT-6 (Met93 of A-chain) and β2M (Asp53 of B chain), highlighting of the hydrogen bond interactions, is shown in pink dotted line, and important residues are shown in stick model: ESAT-6 (green color) and β2M (orange color). The protein structure is represented by chain β2M (orange) and ESAT-6 (green) color. The crucial residues involved in the interaction are circled. (**B**) The interaction is lost when ESAT-6 is docked with β2M–Asp53Ala, displaying the residues that moved away from the C-terminal region of ESAT-6 because of the mutation in β2M. (**C**) Distance plot for Asp53B:N hydrogen bond interaction with Met93A:O in model system 3. (**D**) Superimposition of model system 3 (green) and system 4 (cyan), based on backbone Cα showed RMSD of 5.65 Å. The varied distance between Asp53 of system 3 and mutated Ala53 of system 4 (6.20 Å) is displayed. Crucial residues involved in the interaction are circled.

vector (pGADT7–native β2M or pGADT7–β2M [Asp53Ala]). The pGBKT7–ESAT-6 along with pGADT7–native β2M or pGADT7–β2M (Asp53Ala) were cotransformed in yeast AH109 and were grown in a double-dropout plate deficient in Leu–Trp. Growth of colonies on double-dropout plates was indicative for positive cotransformation, which was further profiled by studying the expression of protein (Fig. 6A) downstream reporter genes (His, Ade, lacZ) grown on a selective media QDO plate. We observed that ESAT-6 could strongly interact with β2M, which was expected (Fig. 6B). However, the strength of this interaction was weaker when ESAT-6 was allowed to interact with the mutant β2M (Asp53Ala). The strength of the interaction was further confirmed by β-gal immunoassay, which indicated a significant decrease (68%) in β-gal concentration for the ESAT-6:β2M (Asp53Ala) when compared with the β-gal concentration for ESAT-6:β2M (Fig. 6C). A plasmid encoding a fusion protein cotransformed with the empty vector did not induce the expression of reporter (His, Ade, lacZ) genes in the AH109 strain grown on QDO selective media.

Prioritization of the small molecules against ESAT-6

Our in silico studies indicated that Asp53 of the β2M molecule exhibits strong hydrogen bond interaction with Met93 of ESAT-6 C-terminal region. The effect of the ESAT-6 molecule on down-regulation of MHC class I Ag presentation by binding to β2M could be rescued by compounds that have strong binding affinity to the C terminus sequence (VTGMFA) of ESAT-6, which is crucial for its interaction with the β2M. Hence, a grid around the crucial residues at the C-terminal region of ESAT-6 was designed for molecular docking-based virtual screening of the databases. A total of 2950 compounds were subjected to docking-based HTVS to discover strong binders of ESAT-6. A cut-off value <-7.0 in Glide XP docking score, crucial residue interactions, and ADME properties were considered for further prioritization. Seventeen molecules, of which three were new moieties from GlaxoSmithKline and 14 were U.S. Food and Drug Administration–approved drugs from DrugBank, displayed high binding affinity toward ESAT-6 with <-7.0 docking score (Supplemental Table II).

To identify the lead molecules that have strong interaction with the C-terminal region of ESAT-6 and competitively prevent binding of β2M with ESAT-6, 17 short-listed molecules (SM01–SM17) (Supplemental Table II) with high Glide docking score were analyzed with MST. Labeled ESAT-6 protein at a final concentration of 20 nM was mixed with 5 μM of test compounds (SM01–SM17) in 10 μl and incubated on ice for 10 min. A single point screening with MST was applied to identify potential binders. Binding was defined by a significantly different signal compared with the negative control (DMSO/buffer only). Out of the 17 compounds, SM09 and SM15 showed stronger affinity, and compounds SM01, SM07 and SM12 showed moderate affinity (Fig. 7A). SM09 and SM15 displayed good signal/noise ratio and amplitude against the control: hence, these

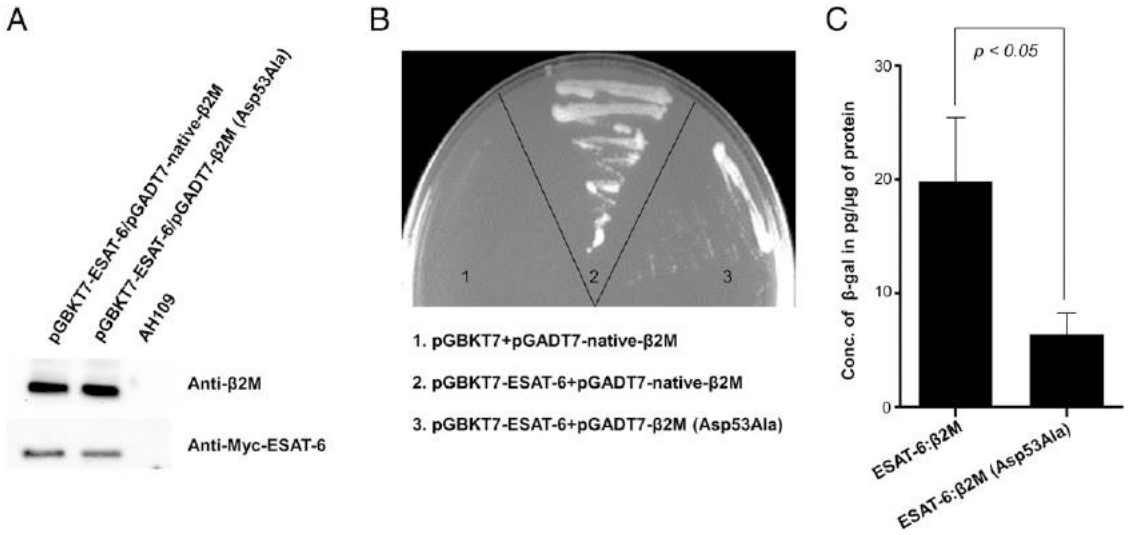

FIGURE 6. Asp53 residue of β2M is crucial for interaction with ESAT-6. A yeast two-hybrid assay was performed to examine the interaction between ESAT-6 and native β2M or mutant β2M (Asp53Ala). Yeast strain AH109 was cotransformed with plasmid encoding ESAT-6 fused with the GAL DNA binding domain pGBKT7–ESAT-6 and β2M fused with the GAL activating domain pGADT7–native β2M or pGADT7–β2M (Asp53Ala) and grown in synthetic dropout media plate (-Ade-His-Leu-Trp). (**A**) Expression of ESAT-6 and β2M in yeast strain AH109 was confirmed by preparing cell lysate expressing either Myc-tag–ESAT-6 and β2M or Myc-tag–ESAT-6 and β2M (Asp53Ala) in Tris buffer, and the lysates were resolved in tricine SDS-PAGE and transferred to nitrocellulose membrane. Myc-tag–ESAT-6 and β2M were detected by Western blotting using rabbit anti-Myc Ab and rabbit anti-β2M Ab. (**B**) Yeast transformed with pGBKT7–ESAT-6 and pGADT7–native β2M showed a higher level of activation of Ade and His reporter gene than pGBKT7–ESAT-6 and pGADT7–β2M (Asp53Ala). pGBKT7–ESAT-6 and pGADT7–native β2M was used as positive control, whereas PGBKT7 and pGADT7–native β2M was used as negative control, which showed no autoactivation of pGBKT7 vector. (**C**). Yeast strain AH109 was cotransformed with pGBKT7–ESAT-6 and pGADT7–native β2M or pGADT7–β2M (Asp53Ala). Yeast strains expressing both bait and prey protein grown on selected media (QDO) and lysate were prepared and incubated in a microplate module coated with anti–β-gal Ab. The β-gal enzyme concentration was detected using a kit from Roche Diagnostics. Data are representative of mean ± SEM of three different experiments.

compounds were further screened for 16-point assay by serial dilution, and data were analyzed using NanoTemper analysis software. These experiments revealed a K_d value of~1.65 μM for the ESAT-6:SM09 complex (Fig. 7B) and~2.83 μM for the ESAT-6:SM15 complex (Fig. 7B). The data suggest existence of a strong interaction between ESAT-6 and compounds (SM09 and SM15) and highlights the affinity for the ESAT-6 C terminus sequence.

Further, the interaction patterns of ESAT-6 protein with SM09 and SM15 were revealed by molecular docking studies followed by MD simulations. SM09 displayed a strong hydrophobic interaction with Met93 and Ala95 along with hydrogen bonding with Gln5 (Fig. 7C). SM15 also exhibited hydrophobic interaction with Met93 and Ile76, including hydrogen bonding with Gln5 and Trp6 (Fig. 7D). The ligand complexes (ESAT-6:SM09 and ESAT-6:SM15) were further subjected for MD simulations, in which RMSD plots for 10 ns displayed stabilized structures; however, conformational deviations were observed in the ligand complexes when compared with a control system (ESAT-6 only) (Fig. 7E). The competitive binding MST experiments of SM09 and SM15 against ESAT-6:β2M complex showed an inhibition with an IC_{50} values of 1.7 and 4.18 μM for SM09 and SM15, respectively (Fig. 7F), and the data obtained are accordance to direct binding experiment.

SM09 and SM15 could rescue cell surface expression of β2M and HLA as well as MHC class I Ag presentation suppressed by ESAT-6

Earlier studies demonstrated that the C-terminal region of ESAT-6 interacts with β2M and sequesters it inside the ER, resulting in decreased cell surface expression of β2M and HLA (17). We next studied whether SM09 and SM15 could rescue cell surface expression of HLA and β2M in the presence of ESAT-6. PMA-differentiated THP-1 macrophages were therefore treated with 12.5 μM of ESAT-6 in the absence or presence of equimolar SM09 or SM15. Cell surface expression of both β2M and HLA was found to be increased in macrophages treated with either ESAT-6:SM09 or ESAT-6:SM15 as compared with ESAT-6 alone (Fig. 8A–D). Cells treated with the inhibitors alone did not have any effect on the surface expression of β2M and HLA.Because SM09 and SM15 interact with ESAT-6 with higher affinity (K_d) compared with β2M (SM09, 1.65 μM; SM15, 2.83 μM; and β2M, 6.9 μM, respectively), these molecules are also likely to rescue ESAT-6–mediated inhibition of MHC class I Ag presentation. To test this hypothesis, peritoneal macrophages from C57BL/6 mice pretreated with recombinant ESAT-6 protein in the absence or presence of SM09 or SM15 were cytosolically loaded with soluble native OVA. The control group received medium or BSA alone. We observed that ESAT-6 downregulated MHC class I Ag presentation, as expected; however, the inhibitory effect of ESAT-6 was rescued in presence of SM09 or SM15 (Fig. 8E). Cells treated with the SM09 and SM15 alone did not affect MHC class I Ag presentation, which was consistent with untreated cells.

Effects of SM09 and SM15 on the survival of M. tuberculosis *inside macrophages*

We next investigated if SM09 or SM15 could affect intracellular survival of *M. tuberculosis* inside macrophages. For this, PMA-differentiated THP-1 macrophages were infected with H37Rv *M. tuberculosis* and cultured in presence of 12.5 μM of either SM09 or SM15 for 12 and 24 h postinfection. Untreated or DMSO-treated macrophages were used as the control. As shown in Fig. 9, the intracellular CFU count was significantly decreased in macrophages treated with these inhibitors as compared with the controls at both the 12- and 24-h time points. These data indicate that both SM09 and SM15 can affect intracellular

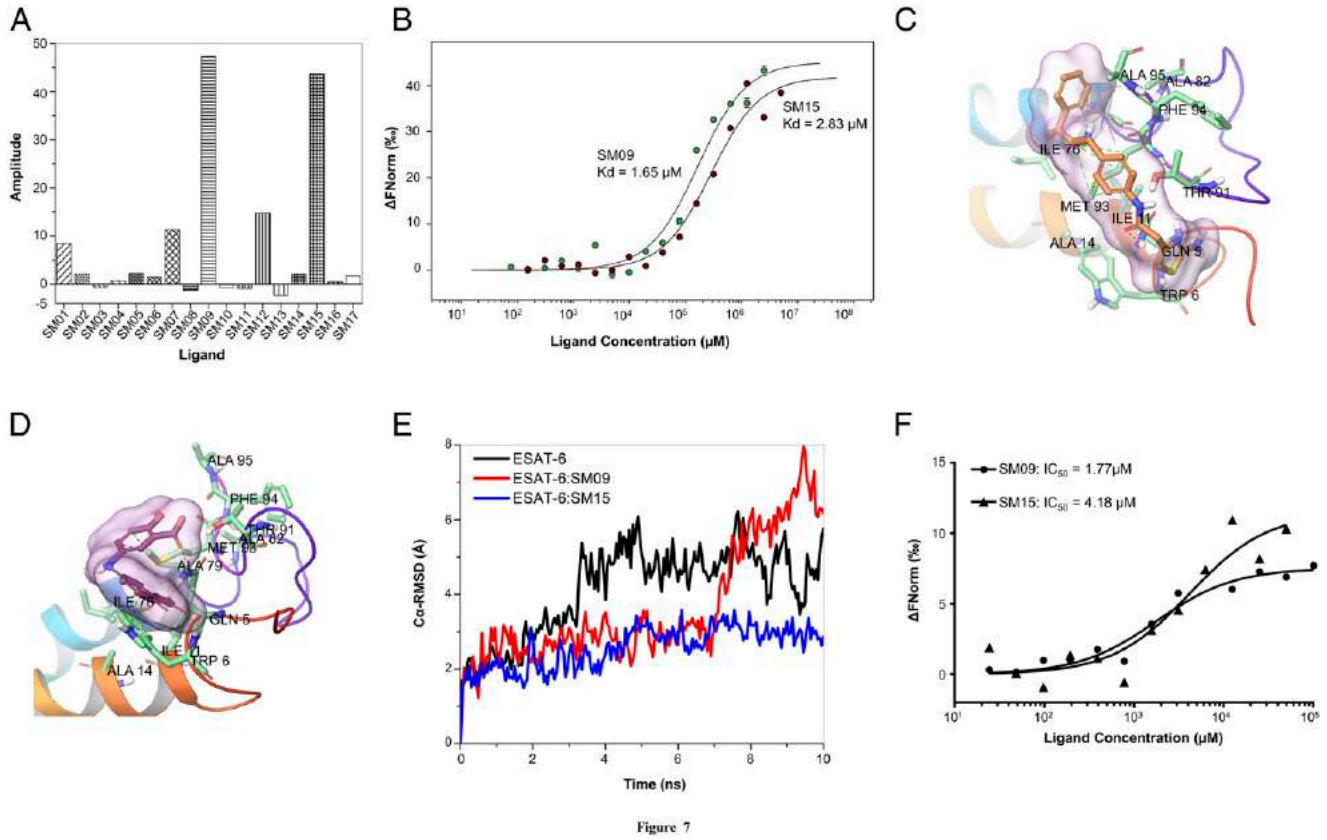

Figure 7

FIGURE 7. Screening of small molecules. (**A**) Single point screening of the docked compounds for identification of the strong binders with ESAT-6 (**B**) MST with the labeled ESAT-6 in the presence of SM09 and SM15 compounds. The change in normalized fluorescence was plotted against the concentration of the serially diluted ligand. A three-dimensional representation of the intermolecular interaction between SM09 (**C**) and SM15 (**D**) with the residues in the ESAT-6 binding pocket during a 10-ns MD simulation. Hydrogen bond interactions are shown in magenta, and the hydrophobic and charged pocket residues are shown in green and purple spheres, respectively. (**E**) The RMSD plot shows the fraction of ESAT-6 and ESAT6:SM09/ESAT-6:SM15 ligand through a 10-ns MD simulation. **(F)** Selectivity profile for SM09 and SM15 as measured by competitive MST assay. ESAT-6:β2M concentration in nanomolar is plotted on the *x*-axis, against changes in normalized fluorescence (ΔF_{norm}) on the *y*-axis. Results shown are representative of three independent experiments.

survival of *M. tuberculosis* and can be potential therapeutic agents against *M. tuberculosis*

Discussion

The ESX-1 of the RD1 region is mostly studied for its well-known set of proteins (ESAT-6 and CFP-10) that are involved in commandeering the host cellular mechanisms. The *M. tuberculosis* ESAT-6 is an important virulence factor that interacts with its chaperone, CFP-10, and is secreted as an ESAT-6:CFP-10 (9, 32). However, in acidic conditions, it dissociates from CFP-10 to interact with the biomembrane of the phagosome (9), theorizing involvement of some host factors in providing stability to ESAT-6 in physiological condition after its dissociation from CFP-10. A recent study from our group has shown that ESAT-6 interacts with the host molecule β2M and inhibits cell surface expression of the MHC class I–β2M complex, resulting in downregulation of MHC class I–mediated Ag presentation (17). Interestingly, ESAT-6 was found to interact with free native β2M but not with β2M in complex with MHC class I. Also, the C-terminal end 6 aa residues (90–95) of ESAT-6 were found to be essential for this interaction. However, the mechanism of ESAT-6:β2M complexation is not fully studied. Hence, it was imperative to understand the ESAT-6:β2M complexation and identify the parameters governing this process. Our multidisciplinary approaches of bioinformatics, biophysics, as well as immunological studies allowed us to determine the strength and pattern of ESAT-6:β2M interaction and to pin down regions of β2M that are involved in interaction with ESAT-6, which is important for identification of new antituberculosis drugs targeting the ESAT-6:β2M complex.

The affinity of ESAT-6 and β2M complex formation revealed a moderate strength of interaction with a K_d = 6.9 μM and stoichiometry of interaction as 1:1. β2M is able to noncovalently interact with other molecules, such as MHC class I, nonclassical MHC class I protein HFE, and MHC class I–like protein CD1, suggesting its vital roles in lipid–Ag presentation and iron homeostasis (18, 20, 21). Church et al. (33) have shown that β2M interacts with HLA with a K_d of 1×10^{-8} M. However, the strength of binding of ESAT-6:β2M is comparatively less than HLA:β2M and ESAT-6:CFP-10 ($K_d = 1.1 \times 10^{-8}$ M) (11, 34). Moreover, in the physiological condition, the concentration of ESAT-6 is decidedly regulated and is probably high; therefore, ESAT-6 is able to bind with free β2M and manipulate macrophage responses (17). ESAT-6:β2M complex is stable at a higher salt concentration and possibly stabilized by hydrophobic interactions (17). To confirm this, we used an ANS binding assay, which revealed that binding of ANS to ESAT-6 was diminished in the ESAT-6:β2M complex when compared with ESAT-6 alone (λ_{max} 521 nm) and showed a red shift at λ_{max} 538 nm. Probably because of molten globule-like structure, ESAT-6 displayed higher binding of ANS in contrast to β2M, which has well-defined globular structure, whereas the ESAT-6:β2M complex was able to bind to a moderate amount of ANS. The decrease in fluorescence intensity of ANS binding to ESAT-6 and red shift at

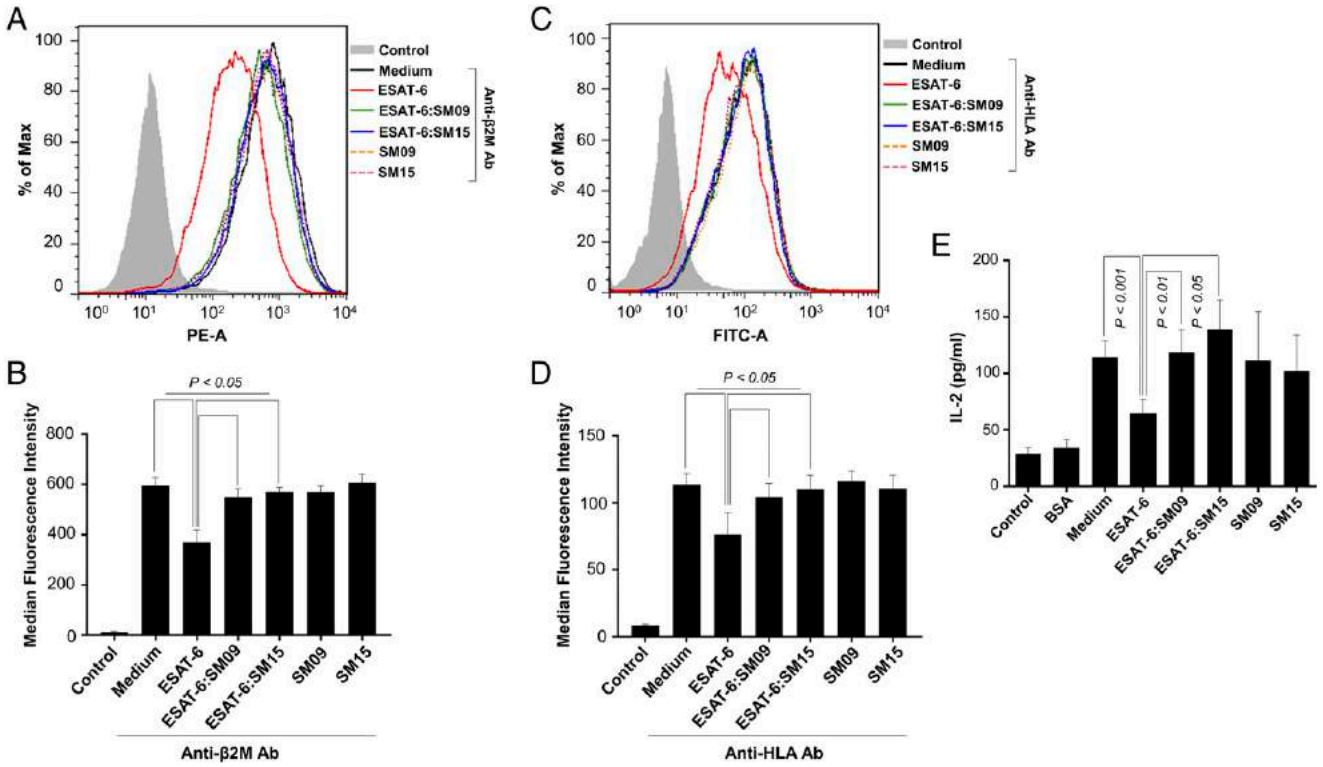

FIGURE 8. SM09 or SM15 rescued surface expression of β2M and HLA as well as MHC class I Ag presentation suppressed by ESAT-6. (**A**–**D**) PMA-differentiated THP-1 macrophages were treated for 2 h with 12.5 μM of recombinant ESAT-6 protein in the absence or presence of equimolar SM09 or SM15 inhibitor. Cells were harvested and incubated with PE-conjugated anti-β2M Ab (A and B) or FITC-conjugated anti-HLA Ab (C and D) for 1 h at 4°C followed by washing with FACS staining buffer, and surface expression of β2M and HLA was analyzed by flow cytometry (A and C). Median fluorescence intensities of different experimental groups described in (A)and (C) were calculated, and the results shown are mean ± SEM of four to five independent experiments (B and D). (**E**) Mice peritoneal macrophages were pretreated with ESAT-6 in the absence or presence of SM09 or SM15 for 2 h. Cells were then cytoplasmically loaded with hypertonic OVA for MHC class I Ag presentation. Next, fixed macrophages were incubated with B3Z T cells. Cells pulsed with hypertonic BSA were used as a control. The levels of IL-2 secreted in the culture supernatants were measured by ELISA. Data are representative of mean ± SEM of three different experiments.

λ_{max} 538 nm in the ESAT-6:β2M complex suggests that the solvent-exposed hydrophobic surface of ESAT-6 is hindered in the presence of β2M. This illustrates that the ESAT-6:β2M complex is stabilized by hydrophobic noncovalent interactions.

Our results demonstrate that conformational changes in β2M occur upon the association of ESAT-6, which might be important to stabilize ESAT-6:β2M complex. ESAT-6 contains three Trp, two Phe, and one Tyr, whereas β2M has three Trp, five Phe, and six Tyr residues (35). β2M has a well-defined β-sandwich Ig fold, which corroborates our near-UV CD spectra results, in which β2M showed a positive peak at 265 and 290 nm. However, after ESAT-6:β2M complexation, a small but significant decrease in the intensity of near-UV spectra was observed, suggesting that the tertiary structure of β2M changes relative to its native conformation. Moreover, ESAT-6 was shown to intrinsically modulate the β2M environment around Trp residues after complex formation. β2M has two Trp residues (Trp60 and Trp95) positioned near to the surface (36), and increasing the concentration of ESAT-6 protein resulted in a decrease in fluorescence intensity. These results clearly indicate that at least one residue of β2M (Trp60 or Trp95) after interaction with ESAT-6 is exposed to a less hydrophobic region and showed a red shift after complex formation with ESAT-6. A study by Raimondi et al. (37) also suggests that Trp95 is essential for folding stability, whereas Trp60, which is solvent exposed, plays a crucial role in promoting the binding of β2M to the H chain of the MHC class I complex (36), which corroborates our findings. Also, our computational results showed the conformational changes across the MD simulations and the importance of noncovalent interactions between β2M and ESAT-6 for their thermal stability (Supplemental Table I). Moreover, the endothermic nature of the interaction of ESAT-6 and β2M and conformational changes in β2M structure upon interaction with ESAT-6 further illustrate that the stability of the complex might be affected. To substantiate the above hypothesis, the stability of the ESAT-6:β2M complex was examined by calculating the ellipticity and the midpoint of the thermal transition as a function of temperature. Our results demonstrate that ESAT-6 in the complex may be stabilized by β2M. The binding of the thermally stable β2M to ESAT-6 might contribute to the stabilization of ESAT-6 in the complex in physiological conditions.

Interestingly, the C-terminal region of ESAT-6 (residues 84–95) is free and is not involved in interaction with CFP-10. Earlier, we established that the last 6 aa (VTGMFA) of the C-terminal region of ESAT-6 are crucial for interaction with free β2M (17). In normal cells, β2M is noncovalently linked with the α-chain polypeptide of the MHC class I– like molecules MHC I/HLA and CD1 and the nonclassical MHC class I protein HFE and makes extensive contacts with all three domains of the α-chain (38) to form a complex. Association of β2M with the α-chain of MHC I, CD1 and HFE is a prerequisite for the cell surface expression of these receptors, and a number of residues at the points of contact with β2M are shared among MHC class I–like molecules, suggesting a common contact among these molecules (38). The residues of β2M that are critical for interaction with ESAT-6 have not been dissected previously, which is an important point of consideration for future discovery of novel drugs. The MD simulation

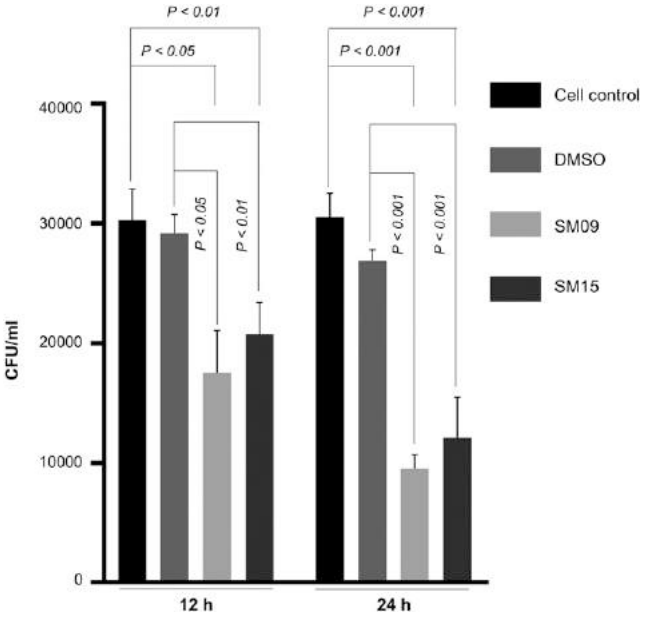

FIGURE 9. SM09 or SM15 affects intracellular survival of *M. tuberculosis* inside the macrophages. PMA-differentiated THP-1 macrophages were infected with H37Rv *M. tuberculosis* strain at multiplicity of infection 1:10 for 4 h, and extracellular bacteria were killed by incubating the cells in medium containing amikacin acid for 2 h. Next, THP-1 macrophages were incubated in fresh medium containing 12.5 μM of SM09 or SM15 for 12- and 24-h time points. Cells were lysed in 0.06% SDS, and bacterial CFUs were counted on 7H11 agar plates. Data shown are mean ± SEM of three independent experiments.

followed by the yeast two-hybridization assay was therefore used to identify the β2M regions that are crucial for interaction with ESAT-6. The human β2M protein structure contains seven aspartate residues (Asp53, Asp59, Asp76, Asp96, and Asp98) that are almost 100% conserved in all the sequences analyzed, whereas Asp34 and Asp38 are found substituted mostly by glutamate or by other polar-uncharged amino acids. The Asp53 residue of β2M is shown to be vital for the stabilization of the MHC class I H chain and β2M complex (39); however, in the isolated β2M, it is totally solvent exposed and devoid of interactions with neighboring residues (40). Asp53 lies in the middle of the β2M D-strand, one of the strands of the four-stranded β-sheet, creating a structural flexibility to harbor the MHC class I H chain. Our computational and site-directed mutagenesis studies clearly suggest that mutation of Asp53Ala in β2M significantly affects the ability of ESAT-6 to form a complex with β2M. Also, our previous results clearly indicated that ESAT-6 can suppress the levels of HLA:β2M complex formation and thereby interfere with MHC class I Ag presentation, eventually, by binding to portions of the available free β2M pool before it forms a complex with the HLA H chain (17). This suggests that Asp53 residue of β2M is required for interaction with both MHC I and ESAT-6. Therefore, ESAT-6 competitively inhibits interaction of β2M with HLA (Supplemental Fig. 1B).

As a well-established virulence factor of *M. tuberculosis*, ESAT-6 is known to undermine protective host immune functions by employing several mechanisms, including interaction with β2M to inhibit Ag presentation (17). In this study, we discovered that ESAT-6 interacts through Asp53 of β2M, an important residue involved in interaction with HLA, HFE, and CD1. Hence, molecules that can specifically mask the β2M interaction site of ESAT-6 would allow rescue from ESAT-6–mediated inhibition of MHC class I Ag presentation. Thus, our findings might help in the designing of drugs for tuberculosis treatment that would target ESAT-6:β2M interaction without affecting MHC:β2M pairing and MHC class I Ag presentation. Hence, we screened for compounds that have a higher affinity for the ESAT-6 protein (especially the C terminus sequence) from various databases through docking-based HTVS. The compounds with the high Glide score were further characterized by analyzing their binding affinity through single point screening on MST. Among 17 potential candidates, SM01, SM07, SM09, SM12, and SM15 exhibited higher affinity to ESAT-6. Out of these molecules, SM09 and SM15 displayed the highest amplitude and strongest affinity for ESAT-6. Both of these compounds were able to rescue ESAT-6–mediated downregulation of cell surface expression of HLA and β2M as well as MHC class I Ag presentation of macrophages. Interestingly, the inhibitors induced a potent inhibitory effect on the survival of *M. tuberculosis* inside macrophages. Thus, SM09 and SM15 appear to be promising drug candidates to improve host protective immunity during tuberculosis infection.

In summary, our study elucidates a comprehensive characterization of ESAT-6:β2M complexation and also enlightens our understanding of the mechanistic process of complexation by identifying the residues that participate in the interaction. The results suggest that ESAT-6 and β2M complexation has moderate affinity stabilized by hydrophobic interfaces and leads to substantial changes in β2M conformation and enhanced thermodynamic stability of ESAT-6 in the complex. Further, mapping of the vital residues involved in the complexation process and identification of the compounds that salvage the effect of ESAT-6 protein on MHC class I Ag presentation, not only shed light on the host–pathogen relationship but also opens up avenues for the development of drugs and therapeutics against tuberculosis.

Acknowledgments

We thank Dr. Yogendra Sharma and the Director of the Centre for Cellular and Molecular Biology (CCMB), Hyderabad, India, for allowing the use of the instrumentation facility of CCMB for the current study. The authors also thank Uday Kiran, Dr. Sivaramaiah Nallapetta (NanoTemper Technologies, Germany), Dr. Madhu Babu Battu, and Dr. Gourango Pradhan for the intellectual interactions and Niteen Pathak for technical help.

Disclosures

The authors have no financial conflicts of interest.

References

1. Pym, A. S., P. Brodin, L. Majlessi, R. Brosch, C. Demangel, A. Williams, K. E. Griffiths, G. Marchal, C. Leclerc, and S. T. Cole. 2003. Recombinant BCG exporting ESAT-6 confers enhanced protection against tuberculosis. *Nat. Med.* 9: 533–539.
2. Lewis, K. N., R. Liao, K. M. Guinn, M. J. Hickey, S. Smith, M. A. Behr, and D. R. Sherman. 2003. Deletion of RD1 from *Mycobacterium tuberculosis* mimics bacille Calmette-Guérin attenuation. *J. Infect. Dis.* 187: 117–123.
3. Guinn, K. M., M. J. Hickey, S. K. Mathur, K. L. Zakel, J. E. Grotzke, D. M. Lewinsohn, S. Smith, and D. R. Sherman. 2004. Individual RD1-region genes are required for export of ESAT-6/CFP-10 and for virulence of *Mycobacterium tuberculosis*. *Mol. Microbiol.* 51: 359–370.
4. Mustafa, A. S., P. J. Cockle, F. Shaban, R. G. Hewinson, and H. M. Vordermeier. 2002. Immunogenicity of *Mycobacterium tuberculosis* RD1 region gene products in infected cattle. *Clin. Exp. Immunol.* 130: 37–42.
5. Gao, L. Y., S. Guo, B. McLaughlin, H. Morisaki, J. N. Engel, and E. J. Brown. 2004. A mycobacterial virulence gene cluster extending RD1 is required for cytolysis, bacterial spreading and ESAT-6 secretion. *Mol. Microbiol.* 53: 1677–1693.
6. Stanley, S. A., S. Raghavan, W. W. Hwang, and J. S. Cox. 2003. Acute infection and macrophage subversion by *Mycobacterium tuberculosis* require a specialized secretion system. *Proc. Natl. Acad. Sci. USA* 100: 13001–13006.
7. Pallen, M. J. 2002. The ESAT-6/WXG100 superfamily -- and a new gram-positive secretion system? *Trends Microbiol.* 10: 209–212.
8. Brodin, P., M. I. de Jonge, L. Majlessi, C. Leclerc, M. Nilges, S. T. Cole, and R. Brosch. 2005. Functional analysis of early secreted antigenic target-6, the dominant T-cell antigen of *Mycobacterium tuberculosis*, reveals key residues

involved in secretion, complex formation, virulence, and immunogenicity. *J. Biol. Chem.* 280: 33953–33959.
9. de Jonge, M. I., G. Pehau-Arnaudet, M. M. Fretz, F. Romain, D. Bottai, P. Brodin, N. Honoré, G. Marchal, W. Jiskoot, P. England, et al. 2007. ESAT-6 from *Mycobacterium tuberculosis* dissociates from its putative chaperone CFP-10 under acidic conditions and exhibits membrane-lysing activity. *J. Bacteriol.* 189: 6028–6034.
10. Wards, B. J., G. W. de Lisle, and D. M. Collins. 2000. An esat6 knockout mutant of *Mycobacterium bovis* produced by homologous recombination will contribute to the development of a live tuberculosis vaccine. *Tuber. Lung Dis.* 80: 185–189.
11. Renshaw, P. S., P. Panagiotidou, A. Whelan, S. V. Gordon, R. G. Hewinson, R. A. Williamson, and M. D. Carr. 2002. Conclusive evidence that the major T-cell antigens of the *Mycobacterium tuberculosis* complex ESAT-6 and CFP-10 form a tight, 1:1 complex and characterization of the structural properties of ESAT-6, CFP-10, and the ESAT-6*CFP-10 complex. Implications for pathogenesis and virulence. *J. Biol. Chem.* 277: 21598–21603.
12. Renshaw, P. S., K. L. Lightbody, V. Veverka, F. W. Muskett, G. Kelly, T. A. Frenkiel, S. V. Gordon, R. G. Hewinson, B. Burke, J. Norman, et al. 2005. Structure and function of the complex formed by the tuberculosis virulence factors CFP-10 and ESAT-6. *EMBO J.* 24: 2491–2498.
13. Okkels, L. M., E. C. Müller, M. Schmid, I. Rosenkrands, S. H. Kaufmann, P. Andersen, and P. R. Jungblut. 2004. CFP10 discriminates between non-acetylated and acetylated ESAT-6 of *Mycobacterium tuberculosis* by differential interaction. *Proteomics* 4: 2954–2960.
14. Houben, D., C. Demangel, J. van Ingen, J. Perez, L. Baldeón, A. M. Abdallah, L. Caleechurn, D. Bottai, M. van Zon, K. de Punder, et al. 2012. ESX-1-mediated translocation to the cytosol controls virulence of mycobacteria. *Cell. Microbiol.* 14: 1287–1298.
15. Ganguly, N., P. H. Giang, C. Gupta, S. K. Basu, I. Siddiqui, D. M. Salunke, and P. Sharma. 2008. Mycobacterium tuberculosis secretory proteins CFP-10, ESAT-6 and the CFP10:ESAT6 complex inhibit lipopolysaccharide-induced NF-kappaB transactivation by downregulation of reactive oxidative species (ROS) production. *Immunol. Cell Biol.* 86: 98–106.
16. Pathak, S. K., S. Basu, K. K. Basu, A. Banerjee, S. Pathak, A. Bhattacharyya, T. Kaisho, M. Kundu, and J. Basu. 2015. Corrigendum: direct extracellular interaction between the early secreted antigen ESAT-6 of *Mycobacterium tuberculosis* and TLR2 inhibits TLR signaling in macrophages. *Nat. Immunol.* 16: 326.
17. Sreejit, G., A. Ahmed, N. Parveen, V. Jha, V. L. Valluri, S. Ghosh, and S. Mukhopadhyay. 2014. The ESAT-6 protein of *Mycobacterium tuberculosis* interacts with beta-2-microglobulin (β2M) affecting antigen presentation function of macrophage. *PLoS Pathog.* 10: e1004446.
18. Bjorkman, P. J., M. A. Saper, B. Samraoui, W. S. Bennett, J. L. Strominger, and D. C. Wiley. 1987. Structure of the human class I histocompatibility antigen, HLA-A2. *Nature* 329: 506–512.
19. Edidin, M. 1987. The natural history of the major histocompatibility complex: jan klein, john wiley & sons, 1986. £90.75 (xix + 775 pages) ISBN 0 471 80953 5. *Immunol. Today* 8: 159–160.
20. Feder, J. N., A. Gnirke, W. Thomas, Z. Tsuchihashi, D. A. Ruddy, A. Basava, F. Dormishian, R. Domingo, Jr., M. C. Ellis, A. Fullan, et al. 1996. A novel MHC class I-like gene is mutated in patients with hereditary haemochromatosis. *Nat. Genet.* 13: 399–408.
21. Martin, L. H., F. Calabi, F. A. Lefebvre, C. A. Bilsland, and C. Milstein. 1987. Structure and expression of the human thymocyte antigens CD1a, CD1b, and CD1c. *Proc. Natl. Acad. Sci. USA* 84: 9189–9193.
22. Gross, C. N., A. Irrinki, J. N. Feder, and C. A. Enns. 1998. Co-trafficking of HFE, a nonclassical major histocompatibility complex class I protein, with the transferrin receptor implies a role in intracellular iron regulation. *J. Biol. Chem.* 273: 22068–22074.
23. Cohen, N. R., S. Garg, and M. B. Brenner. 2009. Antigen presentation by CD1 lipids, T cells, and NKT cells in microbial immunity. *Adv. Immunol.* 102: 1–94.
24. Ryckaert, J.-P., G. Ciccotti, and H. J. C. Berendsen. 1977. Numerical integration of the cartesian equations of motion of a system with constraints: molecular dynamics of n-alkanes. *J. Comput. Phys.* 23: 327–341.
25. Di Pierro, M., M. L. Mugnai, and R. Elber. 2015. Optimizing potentials for a liquid mixture: a new force field for a tert-butanol and water solution. *J. Phys. Chem. B* 119: 836–849.
26. Tullo, A., G. Mastropasqua, J. C. Bourdon, P. Centonze, M. Gostissa, A. Costanzo, M. Levrero, G. Del Sal, C. Saccone, and E. Sbisà. 2003. Adenosine deaminase, a key enzyme in DNA precursors control, is a new p73 target. *Oncogene* 22: 8738–8748.
27. Seidel, S. A., P. M. Dijkman, W. A. Lea, G. van den Bogaart, M. Jerabek-Willemsen, A. Lazic, J. S. Joseph, P. Srinivasan, P. Baaske, A. Simeonov, et al. 2013. Microscale thermophoresis quantifies biomolecular interactions under previously challenging conditions. *Methods* 59: 301–315.
28. Ahmed, A., K. Dolasia, and S. Mukhopadhyay. 2018. *Mycobacterium tuberculosis* PPE18 protein reduces inflammation and increases survival in animal model of sepsis. *J. Immunol.* 200: 3587–3598.
29. Sanderson, S., and N. Shastri. 1994. LacZ inducible, antigen/MHC-specific T cell hybrids. *Int. Immunol.* 6: 369–376.
30. Moore, M. W., F. R. Carbone, and M. J. Bevan. 1988. Introduction of soluble protein into the class I pathway of antigen processing and presentation. *Cell* 54: 777–785.
31. Karttunen, J., S. Sanderson, and N. Shastri. 1992. Detection of rare antigen-presenting cells by the lacZ T-cell activation assay suggests an expression cloning strategy for T-cell antigens. *Proc. Natl. Acad. Sci. USA* 89: 6020–6024.
32. Champion, M. M., E. A. Williams, R. S. Pinapati, and P. A. Champion. 2014. Correlation of phenotypic profiles using targeted proteomics identifies mycobacterial esx-1 substrates. *J. Proteome Res.* 13: 5151–5164.
33. Church, W. R., M. D. Poulik, and R. A. Reisfeld. 1982. Association of human and bovine β_2-microglobulins with detergent solubilized HLA-A,B antigens. *J. Immunol. Methods* 52: 97–104.
34. Meher, A. K., N. C. Bal, K. V. Chary, and A. Arora. 2006. *Mycobacterium tuberculosis* H37Rv ESAT-6-CFP-10 complex formation confers thermodynamic and biochemical stability. *FEBS J.* 273: 1445–1462.
35. Parker, K. C., and J. L. Strominger. 1982. Sequence of human beta 2-microglobulin: a correction. *Mol. Immunol.* 19: 503–504.
36. Kihara, M., E. Chatani, K. Iwata, K. Yamamoto, T. Matsuura, A. Nakagawa, H. Naiki, and Y. Goto. 2006. Conformation of amyloid fibrils of β_2-microglobulin probed by tryptophan mutagenesis. *J. Biol. Chem.* 281: 31061–31069.
37. Raimondi, S., N. Barbarini, P. Mangione, G. Esposito, S. Ricagno, M. Bolognesi, I. Zorzoli, L. Marchese, C. Soria, R. Bellazzi, et al. 2011. The two tryptophans of β2-microglobulin have distinct roles in function and folding and might represent two independent responses to evolutionary pressure. *BMC Evol. Biol.* 11: 159.
38. Tysoe-Calnon, V. A., J. E. Grundy, and S. J. Perkins. 1991. Molecular comparisons of the β 2-microglobulin-binding site in class I major-histocompatibility-complex α-chains and proteins of related sequences. *Biochem. J.* 277: 359–369.
39. Shields, M. J., N. Assefi, W. Hodgson, E. J. Kim, and R. K. Ribaudo. 1998. Characterization of the interactions between MHC class I subunits: a systematic approach for the engineering of higher affinity variants of beta 2-microglobulin. *J. Immunol.* 160: 2297–2307.
40. de Rosa, M., A. Barbiroli, S. Giorgetti, P. P. Mangione, M. Bolognesi, and S. Ricagno. 2015. Decoding the structural bases of D76N β2-microglobulin high amyloidogenicity through crystallography and Asn-Scan mutagenesis. *PLoS One* 10: e0144061.

The Journal of Immunology

ESAT-6 Protein of *Mycobacterium tuberculosis* Increases Holotransferrin-Mediated Iron Uptake in Macrophages by Downregulating Surface Hemochromatosis Protein HFE

Vishwanath Jha, Ravi Pal, Dhiraj Kumar and Sangita Mukhopadhyay

J Immunol published online 4 November 2020
http://www.jimmunol.org/content/early/2020/11/03/jimmunol.1801357

The Journal of Immunology is published twice each month by
The American Association of Immunologists, Inc.,
1451 Rockville Pike, Suite 650, Rockville, MD 20852

Print ISSN: 0022-1767 Online ISSN: 1550-6606.

Published November 4, 2020, doi:10.4049/jimmunol.1801357

ESAT-6 Protein of *Mycobacterium tuberculosis* Increases Holotransferrin-Mediated Iron Uptake in Macrophages by Downregulating Surface Hemochromatosis Protein HFE

Vishwanath Jha,*,† Ravi Pal,*,† Dhiraj Kumar,‡ and Sangita Mukhopadhyay*

Iron is an essential element for *Mycobacterium tuberculosis*; it has at least 40 enzymes that require iron as a cofactor. Accessibility of iron at the phagosomal surface inside macrophage is crucial for survival and virulence of *M. tuberculosis*. ESAT-6, a 6-kDa-secreted protein of region of difference 1, is known to play a crucial role in virulence and pathogenesis of *M. tuberculosis*. In our earlier study, we demonstrated that ESAT-6 protein interacts with β-2-microglobulin (β2M) and affects class I Ag presentation through sequestration of β2M inside endoplasmic reticulum, which contributes toward inhibition of MHC class I:β2M:peptide complex formation. The 6 aa at C-terminal region of ESAT-6 are essential for ESAT6:β2M interaction. β2M is essential for proper folding of HFE, CD1, and MHC class I and their surface expression. It is known that *M. tuberculosis* recruit holotransferrin at the surface of the phagosome. But the upstream mechanism by which it modulates holotransferrin-mediated iron uptake at the surface of macrophage is not well understood. In the current study, we report that interaction of the ESAT-6 protein with β2M causes downregulation of surface HFE, a protein regulating iron homeostasis via interacting with transferrin receptor 1 (TFR1). We found that ESAT-6:β2M interaction leads to sequestration of HFE in endoplasmic reticulum, causing poorer surface expression of HFE and HFE:TFR1 complex (nonfunctional TFR1) in peritoneal macrophages from C57BL/6 mice, resulting in increased holotransferrin-mediated iron uptake in these macrophages. These studies suggest that *M. tuberculosis* probably targets the ESAT-6 protein to increase iron uptake. *The Journal of Immunology*, 2020, 205: 000–000.

Mycobacterium tuberculosis is an intracellular pathogen that infects the macrophage. Inside macrophage phagosome, the bacilli have access to the holotransferrin, which is an important source of iron. *M. tuberculosis* has at least 40 enzymes that require iron as cofactor (1), and access to iron inside the macrophage is crucial for the survival and virulence of *M. tuberculosis* (2, 3). Mycobacterial GAPDH present on the surface of *M. tuberculosis* interacts with holotransferrin and transport iron-bound holotransferrin inside the bacterial cells in siderophore-independent manner (4).

Region of difference 1 (RD1) of *M. tuberculosis* is known to be important for its pathogenicity and virulence inside the host (5). RD1 encodes two proteins present in the same operon, early secreted antigenic target 6 kDa (ESAT-6), and culture filtrate protein 10 kDa (CFP-10). They interact with each other in 1:1 ratio (6). ESAT-6 alone or in complex with CFP-10 has an important role in RD1-mediated invasion and modulation of host immune response (7). In phagosome, ESAT-6 destabilizes the phagosomal membrane, allowing mycobacteria to escape from the phagosome (8, 9). We previously demonstrated that ESAT-6 is translocated to endoplasmic reticulum (ER), where it interacts with β2M and prevents MHC class I Ag presentation function of macrophages (10). β2M is noncovalently associated with MHC class I and nonclassical MHC class I proteins like HFE and CD1 (11–13). β2M acts like a chaperone and is required for proper folding and surface expression of MHC class I, HFE, and CD1. Thus, interaction of mycobacterial ESAT-6 with β2M probably results in modulation of multiple host functions.

There is regulation of iron uptake inside the mammalian cell, which is predominantly regulated by HFE in association with transferrin receptor 1 (TFR1). HFE is involved in iron homeostasis along with TFR1. HFE in ER requires β2M for its proper folding and surface expression in macrophage. HFE:β2M complex in association with TFR1 forms a stable trimolecular complex and inhibits binding of holotransferrin to TFR1 on the surface of macrophage and other cells (14). Genetic defects associated with the mutation in HFE molecule causes a disease known as human hemochromatosis, which is linked to high iron overload in the parenchymal cell (12), and some evidences indicated that mice deficient in β2M or HFE had iron overload and were more susceptible to *M. tuberculosis* than the wild-type strain (15–17). A recent study has shown that holotransferrin is an essential source of iron for *M. tuberculosis* (2, 4, 18). *M. tuberculosis* has several membrane proteins like mycobactin, GAPDH, and transporter protein irtAB, which can sequester iron directly either from holotransferrin or through secreted siderophore carboxymycobactin and traffic and transport it to the bacterial cytoplasm (4, 19–21).

*Laboratory of Molecular Cell Biology, Centre for DNA Fingerprinting and Diagnostics, Uppal, Hyderabad 500039, Telangana, India; †Graduate Studies, Manipal Academy of Higher Education, Manipal 576104, Karnataka, India; and ‡International Centre for Genetic Engineering and Biotechnology, New Delhi 110067, India

Received for publication October 9, 2018. Accepted for publication October 1, 2020.

This work was supported by grants from the Department of Biotechnology (DBT), the Government of India (BT/PR20669/MED/29/1072/2016 and BT/HRD/35/01/03/2018), grants from the Department of Science and Technology, Science and Engineering Research Board, Government of India (EMR/2016/000644 and CRG/2019/000239), and a Core Grant from the Centre for DNA Fingerprinting and Diagnostics by the DBT to the laboratory of S.M. V.J. is supported by a fellowship from the Indian Council of Medical Research, Government of India. R.P. is supported by a fellowship from the DBT, Government of India.

Address correspondence and reprint requests to Dr. Sangita Mukhopadhyay, Laboratory of Molecular Cell Biology, Centre for DNA Fingerprinting and Diagnostics, Inner Ring Road, Uppal, Hyderabad 500039, Telangana, India. E-mail address: sangita@cdfd.org.in

Abbreviations used in this article: CDFD, Centre for DNA Fingerprinting and Diagnostics; CFP-10, culture filtrate protein 10 kDa; ER, endoplasmic reticulum; ESAT-6, early secreted antigenic target 6 kDa; ESAT-6ΔC, ESAT-6 protein with deletion of 6 aa at the C-terminal end; MDM, monocyte-derived macrophage; MOI, multiplicity of infection; Ni-NTA, Ni-nitrilotriacetic acid; PVDF, polyvinylidene difluoride; RD1, region of difference 1; TFR1, transferrin receptor 1.

But it is not known how *M. tuberculosis* modulates signaling pathway to access nontoxic and soluble iron in the form of holotransferrin from the host. In this study, the impact of ESAT-6:β2M interaction on holotransferrin-mediated iron uptake in macrophage is investigated.

Materials and Methods

Purification of recombinant ESAT-6:CFP-10 and ESAT-6 protein with deletion of 6 aa at the C-terminal end:CFP-10

ESAT-6:CFP-10 and ESAT-6 protein with deletion of 6 aa at the C-terminal end (ESAT-6ΔC):CFP-10 were cloned, expressed, and purified as described earlier (10). In brief, ESAT-6 and ESAT-6ΔC were cloned into the first multiple cloning sites with an N-terminal His-tag, and CFP-10 was cloned into the second multiple cloning sites without any tag in a dual expression pETDuet-1 vector (Novagen EMD). Protein expression was induced by adding isopropyl β-D-1-thiogalactopyranoside to a final concentration of 1 mM in BL21(DE3) bacterial culture and left in a shaker incubator at 37˚C for 5 h. Bacterial cells were then harvested by centrifugation, and the pellet was resuspended in lysis buffer (50 mM Tris-HCl [pH 8], 500 mM NaCl, and 1 mM PMSF). Bacterial cell lysates were incubated with Ni–nitrilotriacetic acid (Ni-NTA) agarose bead for 30 min and washed with wash buffer (50 mM Tris-HCl [pH 8], 500 mM NaCl, and 30 mM imidazole) to remove nonspecifically bound protein. Next, bound protein was eluted with elution buffer (50 mM Tris-HCl [pH 8], 500 mM NaCl, and 300 mM imidazole) as 1-ml fractions. Proteins purified to near homogeneity were analyzed on 16% Tris-Tricine SDS-PAGE gel.

Animals

C57BL/6 mice were maintained at the animal house facility of Vimta Labs, Hyderabad, India, as well as Centre for DNA Fingerprinting and Diagnostics (CDFD), Hyderabad, India. The experimental protocols were approved by and performed as per the guidelines of the Institutional Animal Ethics Committee of Vimta Labs and CDFD.

Isolation and culture of peritoneal macrophages

Peritoneal macrophages from mice were isolated as described earlier (10, 22, 23). In brief, C57BL/6 mice of 5–7 wk old were injected with 1 ml of 4% thioglycolate medium in the peritoneal cavity. After 4 d of injection, mice were sacrificed with CO_2 asphyxiation, and peritoneal exudates cells were harvested. Cells were resuspended and cultured overnight at 37˚C in complete DMEM (HyClone) containing 10% (v/v) heat inactivated FBS (HyClone) and 1× GlutaMAX (Thermo Fisher Scientific), 1× antibiotic–antimycotic (contains penicillin, streptomycin, and amphotericin B [Thermo Fisher Scientific]). The nonadhered cells were washed and removed by aspirating medium, and adhered macrophages were used for further experiments.

Mycobacterial strains

M. tuberculosis wild-type (H37Rv-WT) and ESAT-6–deleted *M. tuberculosis* (H37Rv–ESAT-6–KO) strains were maintained and cultured in the biosafety level 3 facility of International Centre for Genetic Engineering and Biotechnology, New Delhi, India. Mycobacterial strains were grown in Middlebrook 7H9 Broth supplemented with 10% albumin, dextrose, catalase, and NaCl (HiMedia Laboratories) along with 0.2% glycerol (Sigma-Aldrich) and 0.05% Tween 80 (Sigma-Aldrich) (24).

Isolation of monocytes and monocyte-derived macrophages from human PBMCs

Human PBMCs (Lonza) were washed three times with HBSS (HyClone) and resuspended in RPMI 1640 medium containing 10% FBS, 1× antibiotic–antimycotic, 1× GlutaMAX, and 10 mM HEPES. Cells were allowed to adhere to a plastic petri dish for 2 h to harvest monocytes, and nonadhered cells were removed by rinsing with PBS (25). For differentiation of monocytes into macrophages, human PBMCs were cultured in RPMI 1640 (HyClone) medium containing 10% FBS. The monocyte-derived macrophages (MDMs) were purified as described by us earlier (26). Briefly, the adherent cells were washed and incubated for 7 d at 37˚C under 5% CO_2 in fresh RPMI 1640 medium supplemented with 15% FBS. After 7 d, MDMs were harvested for studying surface expression of HFE by flow cytometry.

Infection of mice peritoneal macrophage with M. tuberculosis

Peritoneal macrophages from C57BL/6 mice were seeded in complete DMEM for overnight in 37˚C incubator. Nonadherent cells were removed by washing with incomplete DMEM. Cells were infected for 4 h with either H37Rv-WT or H37Rv–ESAT-6–KO *M. tuberculosis* strain at a multiplicity of infection (MOI) of 1:10 in antibiotic-free complete DMEM medium. Cells were washed and incubated for another 2 or 6 h and harvested for further experiments.

Transient transfection of BMC2 macrophages with pcDNA-β2M

For cloning of β2M, RNA was extracted from THP-1 macrophages and was used for cDNA synthesis using SuperScript Reverse Transcriptase III (Invitrogen). This cDNA was used as templet to amplify β2M gene using specific set of primers (forward primers, 5′-GGAAAAGCTTATGATC-CAGAAAACCCCTCAAATTCAAGTA-3′; reverse primers, 5′-TATATC-TAGATCACATGTCTCGATCCCAGTAGACGGTCTTG-3′). Further, β2M was cloned in pcDNA3.1(+) with N-terminal 3× FLAG tag (pcDNA-β2M) using HINDIII and XbaI restriction enzymes.

BMC2 macrophages were cultured in complete DMEM supplemented with 10% FBS, 1× antibiotic–antimycotic, and 1× GlutaMAX. Cells were transfected with Lipofectamine 2000 transfection reagent (Invitrogen) using the manufacturer's protocol. Briefly, 1 μg of plasmid and 3 μl of Lipofectamine 2000 mixture were diluted separately in Opti-MEM (Invitrogen) and incubated at room temperature. The mixture was then added to BMC2 cells cultured with Opti-MEM (Invitrogen). After 6 h of transfection, cells were replenished with fresh complete DMEM medium. Transfected cells were treated with 12.5 μM ESAT-6:CFP-10, and surface expression of HFE of all the groups was measured by flow cytometry.

Flow cytometry

Peritoneal macrophages from C57BL/6 mice were treated with either 12.5 μM of recombinant ESAT-6:CFP-10 or ESAT-6ΔC:CFP-10 protein. Also, C57BL/6 peritoneal macrophages were infected with either H37Rv-WT or H37Rv–ESAT-6–KO *M. tuberculosis* strain. Cells were washed with PBS buffer and stained with rabbit anti-HFE Ab (Abcam) in staining buffer (1% BSA in 1× PBS containing 0.01% sodium azide [NaN_2]), followed by staining with FITC-conjugated anti-rabbit secondary Ab (Sigma-Aldrich) for 1 h on ice. Cell surface expression of HFE was analyzed by flow cytometry (FACSAria; BD Biosciences).

Confocal microscopy

For studying colocalization of HFE with TFR1 on the macrophage surface, mice peritoneal macrophages were treated with 12.5 μM of either ESAT-6:CFP-10 or ESAT-6ΔC:CFP-10 protein or medium alone (cell control) for 2 h in chamber slides. In another experiment, peritoneal macrophages from C57BL/6 mice were infected with either H37Rv-WT or H37Rv–ESAT-6–KO *M. tuberculosis* strain. Cells were next washed two times with 1× PBS and fixed with 4% paraformaldehyde and costained with rabbit anti-HFE Ab (Abcam) and mouse anti-TFR1 Ab (Thermo Fisher Scientific) in 1× PBS containing 2% BSA, followed by staining with Alexa Fluor 488–conjugated anti-rabbit secondary Ab (Thermo Fisher Scientific) and Alexa Fluor 594–conjugated anti-mouse secondary Ab (Thermo Fisher Scientific). Cells were visualized under an LSM 700 Zeiss confocal microscope (Carl Zeiss Micro-Imaging), and the colocalization coefficient was measured using ZEN 2 (blue edition) Carl Zeiss Microscopy software.

For studying ER localization of HFE, calnexin was used as an ER-resident marker protein and colocalization of HFE, and calnexin was studied by confocal microscope LSM 700. Peritoneal macrophages from C57BL/6 mice were treated with either 12.5 μM ESAT-6:CFP-10 or ESAT-6ΔC:CFP-10 protein or infected with either H37Rv-WT or H37Rv–ESAT-6–KO *M. tuberculosis* strain. Cells were washed two times with 1× PBS and fixed with 4% paraformaldehyde. Further, cells were permeabilized with 0.01% Triton X-100 for 10 min and costained with rabbit anti-HFE Ab and mouse anti-calnexin Ab (Abcam). Cells were visualized under LSM 700 Zeiss confocal microscope (Carl Zeiss Micro-Imaging), and the colocalization coefficient was measured using ZEN 2 (blue edition) Carl Zeiss Microscopy software.

For the holotransferrin-mediated iron uptake assay, holotransferrin was prepared and labeled with FITC based on the published protocol as described elsewhere (27, 28). In brief, FITC was dissolved in bicarbonate buffer (pH 9.2) and incubated with holotransferrin at molar ratio 40:1 in 1× PBS at 4˚C for 8 h. Unconjugated free FITC was removed by dialysis in 1× PBS buffer (pH 7.4) at 4˚C. Peritoneal macrophages from C57BL/6 mice were treated with either 12.5 μM ESAT-6:CFP-10 or ESAT-6ΔC:CFP-10 protein or medium alone (cell control) for 2 h. In another experiment, peritoneal macrophages from C57BL/6 mice were infected for 4 h with either H37Rv-WT or H37Rv–ESAT-6–KO *M. tuberculosis* strain (1:10 MOI). Cells were washed and incubated with 6 μM FITC-labeled

holotransferrin for another 2 h in fresh DMEM with 2% BSA. Cells were washed six times with PBS and fixed with 4% paraformaldehyde. Cells were visualized under LSM 700 Zeiss confocal microscope (Carl Zeiss Micro-Imaging), and the intracellular FITC-labeled holotransferrin was quantified using ZEN 2 (blue edition) Carl Zeiss Microscopy software.

Liquid scintillation counting

Liquid scintillation counting was used to determine holotransferrin-mediated iron uptake inside the macrophage. For this, holotransferrin was prepared by mixing 1 mg of apotransferrin (Sigma-Aldrich) with 0.0075 μmol of $^{55}FeCl_3$ (American Radiolabeled Chemicals) and 0.075 μmol of sodium citrate (Sigma-Aldrich) in 40 mM Tris–hydrochloride buffer (pH 7.4) containing 2 mM sodium carbonate (29). After incubating at room temperature for 45 min on a rotor, dialysis was performed at 4˚C against Tris–hydrochloride buffer until no trace of radioactivity was detected in the buffer. Final dialysis of holotransferrin was done in PBS buffer. Peritoneal macrophages from C57BL/6 mice were treated with either 12.5 μM ESAT-6:CFP-10 or ESAT-6ΔC:CFP-10 protein or medium alone (cell control) for 2 h and then incubated with 6 μM ^{55}Fe-transferrin for another 2 h in incomplete DMEM. Cells were washed with ice-cold buffer (0.15 mM glycine–HCl [pH 3] and 50 mM NaCl) for 3 min to remove cell surface-bound ^{55}Fe-transferrin. Cells were washed four times with ice-cold PBS buffer, lysed using PBS buffer with 1% NP-40. The amount of radiolabeled iron incorporated into the cells was counted using a liquid scintillation counter (PerkinElmer) (29).

Western blotting

For Western blotting experiments, cells were lysed in radioimmunoprecipitation assay buffer (25 mM Tris [pH 7.6], 150 mM NaCl, 1% NP-40, 1% sodium deoxycholate, and 0.1% SDS) containing 1 mM PMSF and 1× protein inhibitor mixture (Roche Diagnostics) as described earlier (30). Whole cell extract was resolved on a 16% Tris-Tricine SDS-PAGE gel and transferred to polyvinylidene difluoride (PVDF) membrane. After the transfer of proteins, PVDF membranes were incubated with either anti-HFE Ab or anti-TRF1 Ab or anti–β-actin Ab, followed by appropriate HRP-conjugated secondary Abs. The membrane-bound HRP was detected by chemiluminescence using ECL kit following the manufacturer's protocol (GE Healthcare).

Pull-down assay

Cell lysates were prepared from peritoneal macrophages obtained from C57BL/6 mice using NP-40 lysis buffer (50 mM Tris-HCl, 150 mM NaCl, 1% NP-40, 1× protease inhibitor mixture [Sigma-Aldrich]). Lysates were incubated with Ni-NTA bound either ESAT-6:CFP-10 or CFP-10 at 4˚C. After 4 h of incubation, Ni-NTA beads were collected and washed three times with PBS. A total of 1× Laemmlli buffer was added to the Ni-NTA beads and heated at 95˚C for 5 min. Further, beads were loaded onto 16% Tris-Tricine SDS-PAGE gel and transferred to PVDF membrane. After the transfer of proteins, PVDF membranes were incubated with either anti-HFE Ab or anti-β2M Ab, followed by HRP-conjugated anti-rabbit and anti-mouse appropriate secondary Ab, respectively. The membrane-bound HRP was detected by chemiluminescence using ECL kit following the manufacturer's protocol (GE Healthcare).

Statistics

Statistical comparisons were made using either Student *t* test or by one-way ANOVA followed by Tukey honestly significant difference tests. Calculations were performed using GraphPad Prism. Any p value < 0.05 was considered to be significant.

Results

ESAT-6 downregulates surface expression of HFE protein in macrophages

ESAT-6, a 6-kDa secretory protein of *M. tuberculosis*, is found to be in complex with CFP-10 (6, 31). In the earlier studies, we have shown that ESAT-6 alone or in complex with CFP-10 (ESAT-6:CFP-10) interacts with β2M and sequesters β2M inside ER (10). ESAT-6 protein with deletion of last 6 aa (VTGMFA) at the C-terminal end (ESAT-6ΔC) fails to interact with β2M, indicating that the last 6 aa at the C-terminal end of ESAT-6 are responsible for its interaction with β2M (10). HFE is a nonclassical MHC class I molecule synthesized in ER and forms complex with β2M (HFE:β2M). β2M is essential for proper folding of HFE and its transport to the cell membrane as β2M:HFE complex (12). Therefore, we hypothesized that ESAT-6/ESAT-6:CFP-10 by interacting and sequestering β2M might directly influence the surface expression of HFE in macrophages. To investigate this, mice peritoneal macrophages were treated with either 12.5 μM of recombinant ESAT-6:CFP-10 or ESAT-6ΔC:CFP-10 protein or medium alone for 2 h in incomplete DMEM and were analyzed for surface expression of HFE by flow cytometry. ESAT-6ΔC:CFP-10 was used as a control protein because ESAT-6ΔC:CFP-10 fails to interact with β2M. We observed that the surface expression of HFE is significantly downregulated in cells treated with ESAT-6:CFP-10 as compared with control cells (cells treated with medium alone) or cells treated with ESAT-6ΔC:CFP-10 (Fig. 1A, 1B). Similar results were obtained in case of human monocytes (Fig. 1C, 1D) and MDMs (Fig. 1E, 1F). Because surface levels of HFE in ESAT-6ΔC:CFP-10–treated cells were similar to that of control cells, ESAT-6, but not CFP-10, was responsible for decreased HFE expression on macrophage surface. To examine if ESAT-6 affects surface expression level of HFE by inhibiting expression of HFE protein levels, total expression of HFE protein was measured in the peritoneal macrophages by Western blotting. For this, peritoneal macrophages from C57BL/6 mice were treated with either ESAT-6:CFP-10 or ESAT-6ΔC:CFP-10 protein or medium alone. After 2 h of protein treatment, cell lysates were prepared and immunoblotted using anti-HFE Ab. The results indicated that protein expression level of HFE remained same in all the three groups (Fig. 1G, 1H). This confirms that ESAT-6 downregulates only the surface levels of HFE. As stated earlier, EAST-6:CFP-10 interacts with β2M; therefore, we wanted to know if ESAT-6:CFP-10 interacts with HFE and downregulates it surface expression. Therefore, lysate prepared from mice peritoneal macrophages were incubated with His-tagged ESAT-6:CFP-10 or CFP-10 protein and pulled down using Ni-NTA beads. Fig. 1I reveals that although ESAT-6:CFP-10 could pull down β2M, which was expected, no band specific to HFE was pulled down along with ESAT-6:CFP-10 or CFP-10. These results clearly indicate that ESAT-6 does not directly interact with HFE but downregulates surface expression of HFE probably through interacting directly with β2M, preventing its complex formation with HFE. As expected (10), CFP-10 did not interact with β2M (Fig. 1I).

Because β2M is essential for proper folding of HFE and its transport to the cell membrane, and because the sequestration of β2M by ESAT-6 is probably responsible for the decreased trafficking of HFE from the ER to the cell surface, we next examined the restoration of surface expression of HFE in β2M-overexpressed cells treated with ESAT-6:CFP-10. For this, BMC2 macrophages were transfected with either pcDNA3.1 vector alone (vector control) or pcDNA-β2M (Fig. 1J) and treated with 12.5 μM ESAT-6:CFP-10. We observed that surface expression of HFE was higher in cells transfected with pcDNA-β2M as compared with cells harboring the vector alone (Fig. 1K, 1L). This study indicates that the effect of ESAT-6 can be reversed by overexpression of β2M.

To confirm further the effect of ESAT-6 on surface expression of HFE during mycobacterial infection, peritoneal macrophages from C57BL/6 mice were infected with either H37Rv-WT or H37Rv–ESAT-6–KO. Cells were stained with rabbit anti-HFE Ab, followed by incubation with FITC-conjugated anti-rabbit secondary Ab, and surface expression of HFE was measured by flow cytometry. As expected, surface expression level of HFE was lower in cells infected with H37Rv-WT, as compared with HFE levels in cells infected with H37Rv–ESAT-6–KO at both 2 (Fig. 2A, 2B)– and 6-h time points (Fig. 2C, 2D).

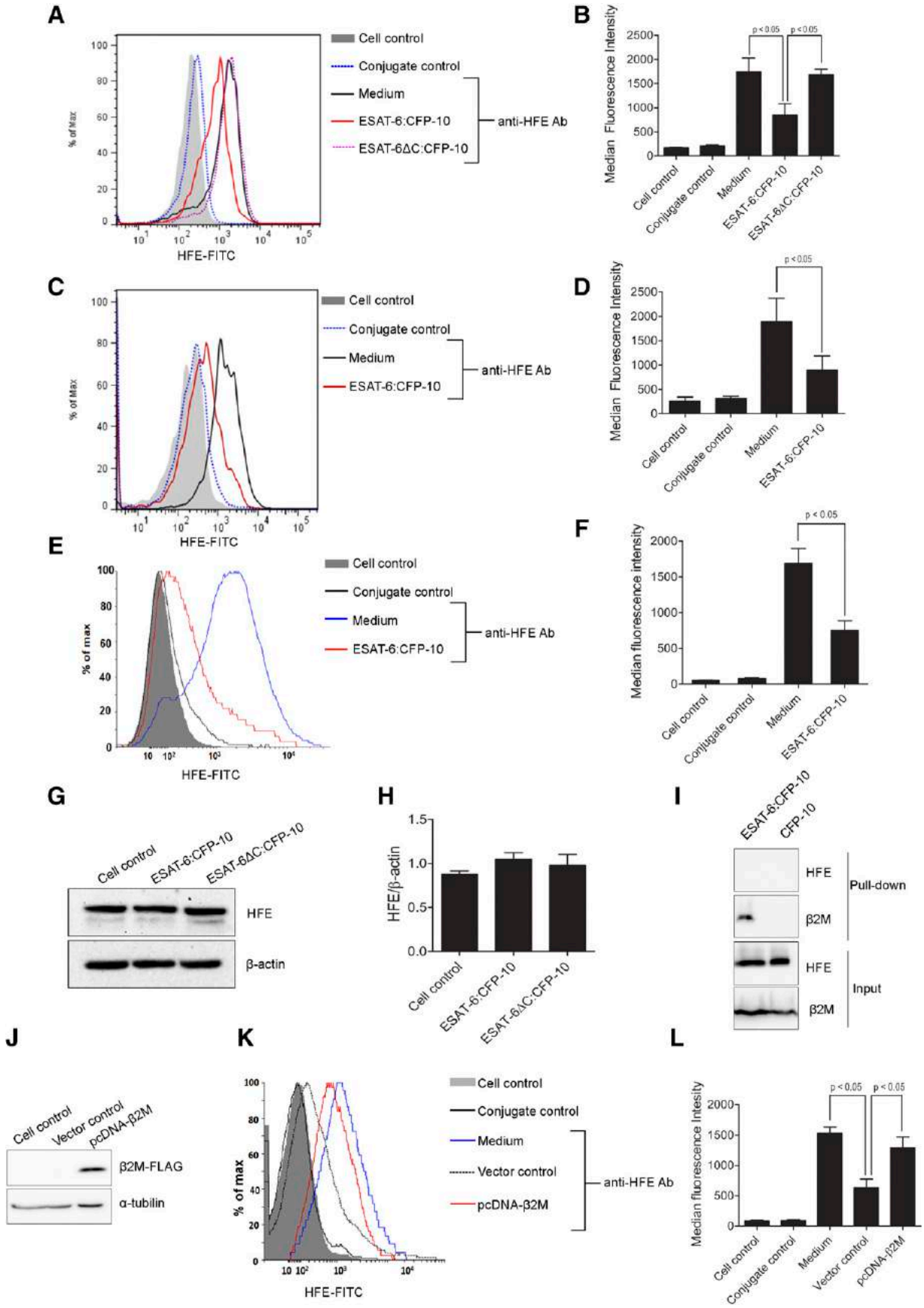

FIGURE 1. Exogenous addition of soluble ESAT-6:CFP-10 protein downregulates surface expression of HFE molecules. Peritoneal macrophages from C57BL/6 mice were treated with 12.5 μM of either ESAT-6:CFP-10 or ESAT-6ΔC:CFP-10 protein (**A** and **B**). The control group received medium alone. Surface expression of HFE was measured by flow cytometry (A). Median fluorescence intensities of different experimental groups were calculated, and the results are shown as mean ± SEM of three independent experiments (B). Human monocytes (**C** and **D**) or MDMs (**E** and **F**) were *(Figure legend continues)*

HFE is accumulated in the ER of cells exposed to ESAT-6

HFE is known to be associated with its chaperone, β2M, which is important for its proper processing, stability, and the expression on the cell surface (12). Earlier studies indicate that ESAT-6:CFP-10 protein is translocated to the ER, where it interacts and sequesters β2M inside the ER (10). Thus, in the presence of ESAT-6, β2M becomes a limiting factor to form complex with HFE and translocation of HFE:β2M to the cell surface. Thus, ESAT-6:β2M interaction may lead to accumulation of the free-form HFE inside ER, where it is synthesized and undergoes posttranslational modification. To understand the effect of ESAT-6:CFP-10 in sequestration of HFE inside ER, confocal microscopy was carried out for studying colocalization of HFE and calnexin (ER-resident marker protein). Peritoneal macrophages from C57BL/6 mice were therefore exogenously treated with either soluble 12.5 μM ESAT-6:CFP-10 or ESAT-6ΔC:CFP-10 protein. After 2 h of protein treatment, cells were fixed in 4% paraformaldehyde and costained with anti-HFE Ab and anti-calnexin Ab, and cells were visualized under confocal microscope. An increased amount of HFE was found to be accumulated in ER of macrophages that were treated with ESAT-6:CFP-10 as compared with ESAT-6ΔC:CFP-10 (Fig. 3A, 3B).

To confirm further the effect of ESAT-6 on HFE accumulation in ER during mycobacterial infection, peritoneal macrophages from C57BL/6 mice were infected with either H37Rv-WT or H37Rv–ESAT-6–KO *M. tuberculosis* strain. Cells were fixed in 4% paraformaldehyde and costained with anti-HFE Ab and anti-calnexin Ab and visualized under confocal microscope. As expected, we observed that macrophages infected with H37Rv-WT had better colocalization of HFE with calnexin as compared with macrophages infected with H37Rv–ESAT-6–KO *M. tuberculosis* strain (Fig 3C, 3D). These results suggest that ESAT-6 helps in retention of HFE in ER in macrophages during protein treatment or infection, which is probably due to unavailability of free β2M molecule to form complex with HFE and its trafficking to the cell surface.

ESAT-6 inhibits the surface accumulation of HFE:TFR1 complex

TFR1 is a glycoprotein present on the surface of most mammalian cells. TFR1 is a central molecule required for iron homeostasis in association with HFE. TFR1 bound to holotransferrin (an iron-bound plasma transport protein) (32) undergoes clathrin-mediated endocytosis and transport iron inside the cells (33, 34). In ER, β2M:HFE complex interacts with TFR1 to form β2M:HFE:TFR1 complex and is trafficked through Golgi to the cell surface (14, 33). β2M:HFE after interacting with TFR1 reduces the binding ability of TFR1 to holotransferrin and inhibits endocytosis of holotransferrin-bound TFR1. When the stable β2M:HFE:TFR1 complex is accumulated at the cell surface, it reduces holotransferrin-mediated iron uptake inside the cells (35). This is a regulation for iron uptake by the normal cell to maintain iron homeostasis. ESAT-6:CFP-10 via interacting with β2M probably limits availability of free β2M to form a complex with HFE. This may affect complex formation with TFR1. Hence, we investigated whether downregulation of surface HFE by ESAT-6:CFP-10 could alter the accumulation of HFE:TFR1 complex at the surface of macrophage. As shown in Fig. 4A and 4B, HFE:TFR1 complexes at the cell surface were downregulated in cells treated with ESAT-6:CFP-10 as compared with cells treated with ESAT-6ΔC:CFP-10 or cells treated with medium alone. The data also indicate presence of more amount of free TFR1 on the surface of cells treated with ESAT-6:CFP-10 than the cells treated with ESAT-6ΔC:CFP-10 or cell control. The Western blots indicate that ESAT-6 does not change the total expression of TFR1 protein (Fig. 4C, 4D). Similar results were obtained when peritoneal macrophages from C57BL/6 mice were infected with either the H37Rv-WT or H37Rv–ESAT-6–KO *M. tuberculosis* strain. Macrophages infected with H37Rv-WT showed lesser HFE:TRF1 complex at the surface as compared with cells infected with H37Rv–ESAT-6–KO strain at both 2- and 6-h time points (Fig. 4E, 4F). All these results precisely indicate that ESAT-6 downregulates surface level of HFE:TFR1 complex in macrophages.

ESAT-6 elevates TFR1–holotransferrin-mediated uptake of iron inside macrophages

It is known that HFE has an important role in intracellular iron regulation along with TFR1. HFE interacts with TFR1 and inhibits TFR1–holotransferrin-mediated iron uptake in cells by decreasing the availability of TFR1 for holotransferrin. Studies in earlier section revealed that treatment of cells with ESAT-6:CFP-10 results in decreased level of HFE:TFR1 complex on the surface of macrophages but increased concentration of free TFR1. Therefore, it is possible that downregulation of HFE by ESAT-6 results in increased holotransferrin-mediated iron uptake through free TFR1. To test this, holotransferrin uptake assay was performed using FITC-labeled holotransferrin. Peritoneal macrophages from C57BL/6 mice were treated with 12.5 μM of either ESAT-6:CFP-10 or ESAT-6ΔC:CFP-10 protein or medium alone. After 2 h of protein treatment, cells were washed with medium and incubated with 6 μM FITC-labeled holotransferrin for another 2 h in 2% BSA in fresh DMEM. Cells were washed with PBS and fixed in 4% paraformaldehyde, and uptake of iron inside the cells was visualized under confocal microscope. Uptake of holotransferrin was found to be increased in cells treated with ESAT-6:CFP-10 as compared with cells treated with ESAT-6ΔC:CFP-10 or control cells (Fig. 5A, 5B). No nonspecific binding of free FITC was observed in buffer control, which was treated with last dialysis buffer. To further confirm the fact that ESAT-6 increases holotransferrin-mediated iron uptake, next radiolabeled holotransferrin (^{55}Fe-transferrin) was used. For this, cells were exogenously treated with 12.5 μM ESAT-6:CFP-10 or ESAT-6ΔC:CFP-10

treated with 12.5 μM of recombinant ESAT-6:CFP-10 protein. The control group received medium alone. Surface expression of HFE was analyzed by flow cytometry (C and E). Median fluorescence intensities of different experimental groups were calculated, and the results are shown as mean ± SEM of three independent experiments (D and F). Mice peritoneal macrophages were treated either with ESAT-6:CFP-10 or ESAT-6ΔC:CFP-10 for 2 h. Level of HFE protein was measured by Western blotting (**G**). Densitometric analyses of the Western blots were carried out using ImageJ software using β-actin as loading control (**H**). Results shown are mean ± SEM of three independent experiments. In another experiment, lysates prepared from peritoneal macrophages from C57BL/6 mice were incubated with Ni-NTA–bound ESAT-6:CFP-10 or CFP-10, and the pull-down product was immunoblotted with anti-HFE Ab or anti-β2M Ab. The protein bands were visualized by chemiluminescence (**I**). BMC2 macrophages were treated with medium alone or transiently transfected with either pcDNA3.1 (vector control) or pcDNA3.1 harboring β2M gene (pcDNA-β2M). β2M overexpression was checked by Western blotting using anti-FLAG Ab (**J**). Transfected cells were treated with ESAT-6:CFP-10 and surface expression of HFE of all the groups (medium, vector control, and pcDNA-β2M) was measured by flow cytometry (**K**). Median fluorescence intensities of different experimental groups were calculated, and the results are shown as mean ± SEM of three independent experiments (**L**).

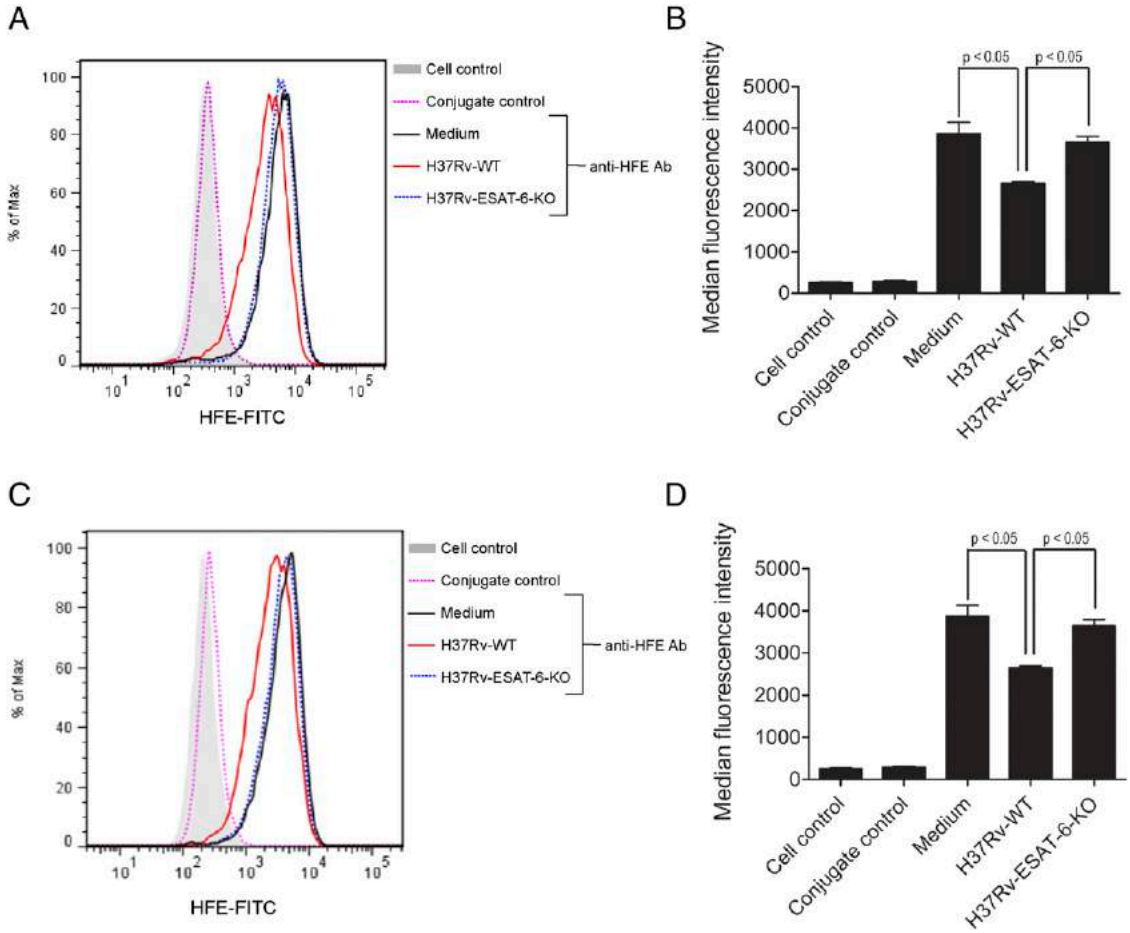

FIGURE 2. ESAT-6 downregulates surface expression of HFE in macrophages during infection with *M. tuberculosis*. Peritoneal macrophages from C57BL/6 mice were either infected with H37Rv-WT or H37Rv–ESAT-6–KO *M. tuberculosis* strain. After 2 h (**A** and **B**) and 6 h (**C** and **D**), surface expression of HFE was analyzed by flow cytometry. Median fluorescence intensities of different experimental groups were calculated, and the results were shown as mean ± SEM of four independent experiments (B and D). Uninfected cells were used as control.

or medium alone and then incubated with 6 μM ^{55}Fe-transferrin. The amount of radiolabeled intracellular iron uptake was measured using liquid scintillation counter. As shown in Fig. 5C, level of intracellular iron was found to be more in cells treated with ESAT-6:CFP-10 as compared to cells treated with ESAT-6ΔC:CFP-10 or control cells. All these observations demonstrate that ESAT-6:CFP-10 increases holotransferrin-mediated uptake of iron in macrophages. When TFR1 holotransferrin-mediated iron uptake was determined in macrophages infected with either H37Rv-WT or H37Rv–ESAT-6–KO, intracellular level of holotransferrin-bound iron was found to be higher in cells infected with H37Rv-WT than cells infected with H37Rv–ESAT-6–KO strain (Fig. 6). This observation suggests that *M. tuberculosis* targets the ESAT-6 protein to increase the intracellular iron level during infection.

Discussion

Iron is an important element required by all organisms for regulating various biological processes. The virulence property of a pathogen depends upon the availability of iron; hence, there is a quest for iron by the pathogen in host cells. In human, iron is absorbed in the duodenum and transported to the macrophage by iron-bound plasma transport protein, transferrin through TFR–transferrin pathway. *M. tuberculosis* resides in phagosome that has limited access to iron (36, 37). In several studies, it has been shown that iron overload leads to increase in susceptibility to *M. tuberculosis* infection (16, 17, 38). It was also found that mice deficient in β2M or HFE became prone to *M. tuberculosis* infection (16, 17). HFE is a nonclassical MHC class I protein and has a similar structure to MHC class I; however, the Ag-binding groove is smaller in HFE than MHC class I and is not involved in Ag presentation (32, 34). It is observed that HFE along with TFR1 has an important role in iron homeostasis in macrophage (33). HFE–TFR1 complex remains associated at the cell surface and inhibits holotransferrin-mediated iron uptake (35). In the current study, we have shown that the mycobacterial protein ESAT-6 modulates surface expression of HFE and subsequently affects holotransferrin-mediated iron uptake. ESAT-6/ESAT-6:CFP-10 manipulates many host factors in macrophage and hijacks the host immune system to make a safe niche for the bacilli to survive inside the macrophages. It has been reported earlier that ESAT-6 plays a crucial role in supporting intracellular growth of the bacilli in host (5, 7, 39–44). In the previous study, we have demonstrated that ESAT-6 alone or in complex with CFP-10 (ESAT-6:CFP-10) interacts with β2M, and the C-terminal end of ESAT-6 is crucial for its interaction with β2M as ESAT-6 protein with deletion of 6 aa in the C-terminal end failed to interact with β2M (10). Thus, ESAT-6, but not CFP-10, is involved in the complex formation with β2M and modulation of macrophage effectors function associated with β2M. In this study, we have shown that ESAT-6:CFP-10 downregulates surface expression of HFE. Surface expression of HFE was also lower in macrophages infected with H37Rv-WT *M. tuberculosis* as compared with HFE in macrophages infected with H37Rv–ESAT-6–KO *M. tuberculosis* strain. These results suggest that *M. tuberculosis* targets

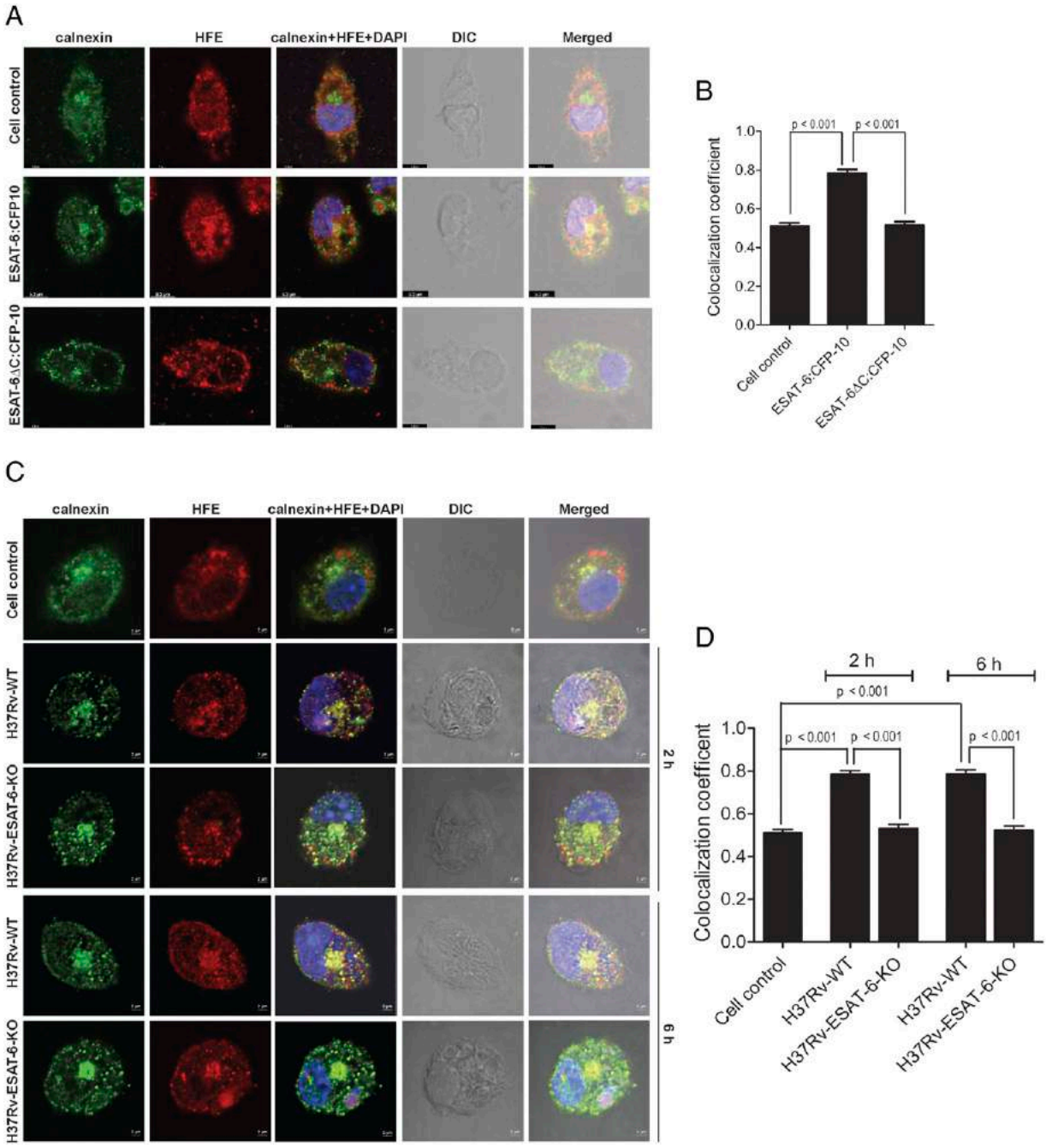

FIGURE 3. ESAT-6 accumulates HFE in ER of macrophages. Peritoneal macrophages form C57BL/6 mice were treated with either ESAT-6:CFP-10 or ESAT-6ΔC:CFP-10 protein. The control group received medium alone. After 2 h of protein treatment, cells were fixed, permeabilized, and costained with anti-HFE Ab and anti-calnexin Ab. Colocalization of HFE (red) with calnexin (green) was observed under confocal microscope (**A**). Colocalization coefficient was measured and shown as mean ± SEM from 50 cells of three independent experiments (**B**). In another experiment, peritoneal macrophages form C57BL/6 mice were infected with either H37Rv-WT or H37Rv–ESAT-6–KO *M. tuberculosis* strain at MOI of 1:10. Cells were fixed, permeabilized, and costained with anti-HFE Ab and anti-calnexin Ab. Colocalization of calnexin (green) with HFE (red) was observed under confocal microscope (**C**). DAPI was used to stain the nucleus. Uninfected cells were used as control. Colocalization coefficient was measured and shown as mean ± SEM from 50 cells of three independent experiments (**D**).

the ESAT-6 protein predominantly to inhibit surface expression of HFE molecules.

β2M acts as the chaperone for HFE and is involved in proper folding and surface expression of HFE (45). ESAT-6 interacts with free β2M and sequesters it inside ER, thus poorer amount of free β2M is available to interact with HFE. This affects proper folding and trafficking of HFE molecules to the surface. Also, it was confirmed that ESAT-6 does not interact directly with HFE and only affects the surface expression of HFE but not its total expression.

HFE is expressed in all the cells, but the expression level of HFE is higher in monocytes, macrophages, granulocytes, and epithelial cells. Hereditary hemochromatosis is an autosomal recessive disorder associated with iron overload in the parenchymal cells, which results in damage of vital organs like liver, heart, and pancreas (46–48). Hereditary hemochromatosis is primarily caused by a point mutation cysteine to tyrosine (C282Y) in HFE (12, 49). This mutation affects HFE–β2M interaction and, therefore, retains HFE in ER and middle Golgi apparatus. Because

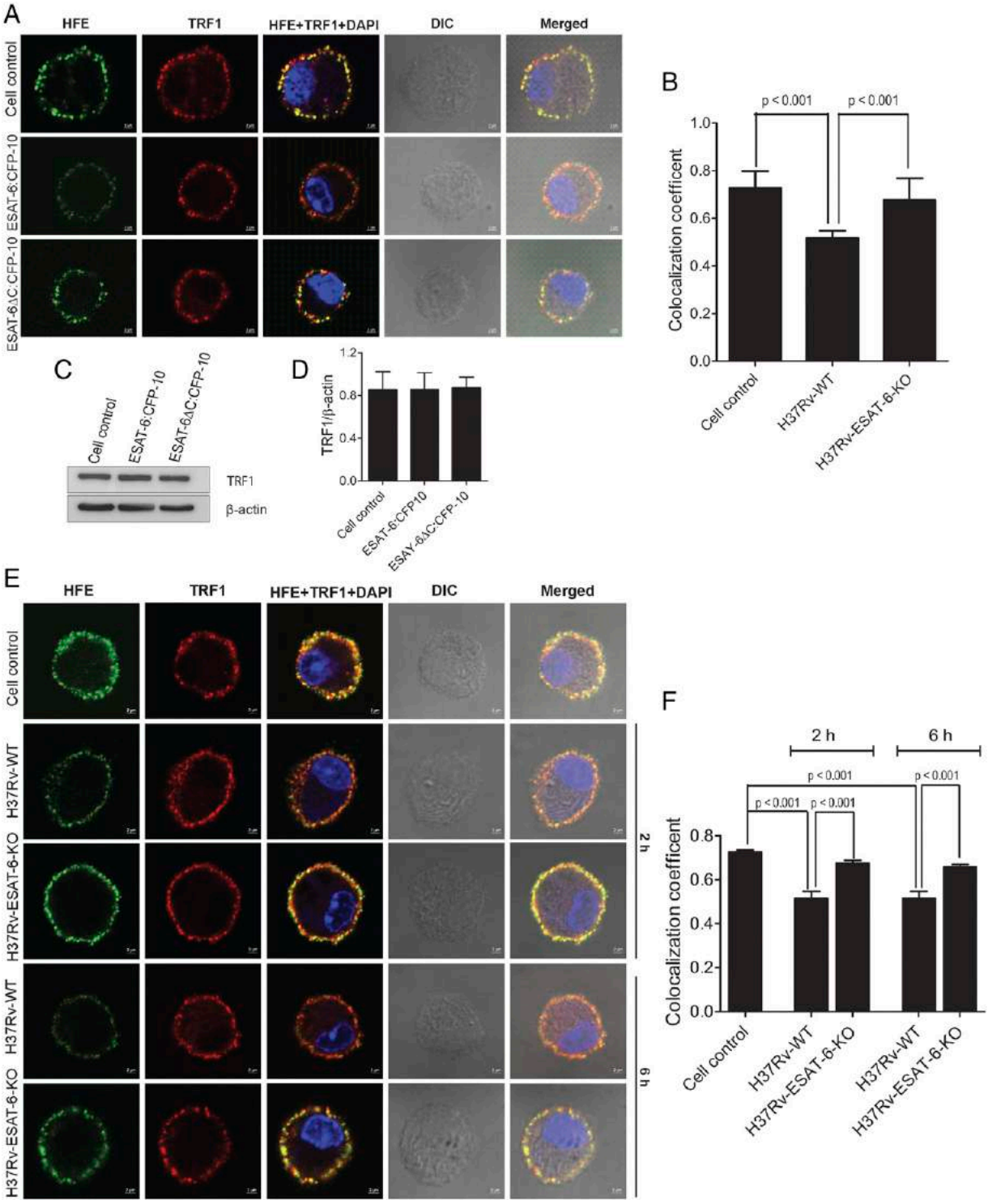

FIGURE 4. ESAT-6 downregulates accumulation of HFE:TFR1 complex at the surface of macrophages. Peritoneal macrophages form C57BL/6 mice were either treated with ESAT-6:CFP-10 or ESAT-6ΔC:CFP-10 protein. The control group received medium alone. After 2 h of protein treatment (**A** and **B**), cells were fixed in paraformaldehyde without permeabilizing it and costained with anti-HFE Ab and anti-TFR1 Ab. Colocalization of HFE (green) with TRF1 (red) was observed under confocal microscope (A). Colocalization coefficient was measured and shown as mean ± SEM from 50 cells of three independent experiments (B). Level of TRF1 protein was measured by Western blotting using anti-TFR1 Ab (**C**), and densitometric analyses of the Western blots were carried out using ImageJ software using β-actin as loading control (**D**). Results shown are mean ± SEM of three independent experiments. Peritoneal macrophages from C57BL/6 mice were infected with either H37Rv-WT or H37Rv–ESAT-6–KO *M. tuberculosis* strain at MOI of 1:10. Cells were fixed in paraformaldehyde without permeabilizing and costained with anti-HFE Ab and anti-TRF1 Ab. Colocalization of HFE (green) with TRF1 (red) was observed under confocal microscope (**E**). DAPI was used to stain the nucleus. Uninfected cells were used as control. Colocalization coefficient was measured and shown as mean ± SEM from 50 cells of three independent experiments (**F**).

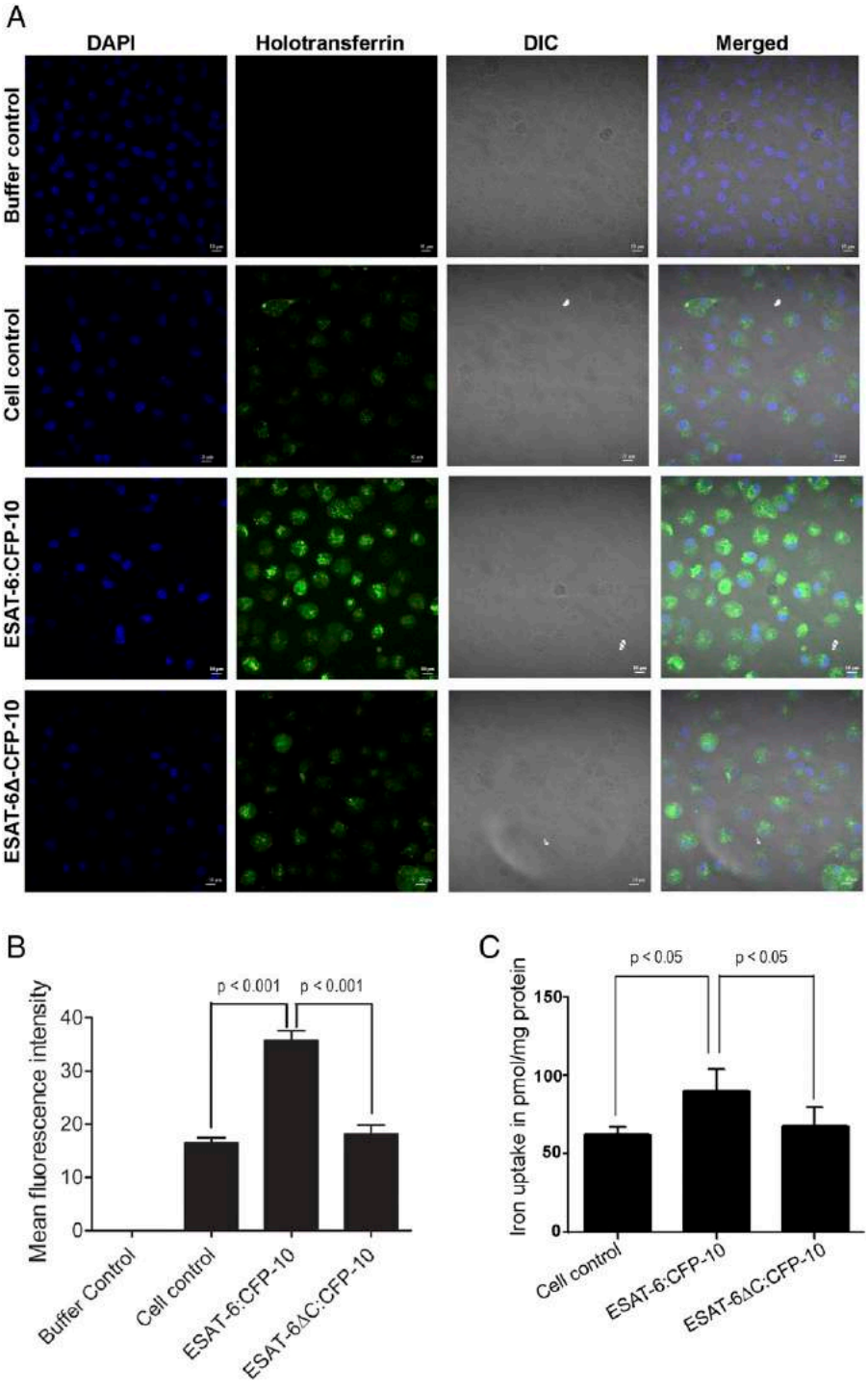

FIGURE 5. ESAT-6:CFP-10 increases holotransferrin-mediated uptake of iron inside macrophages. Peritoneal macrophages form C57BL/6 mice were treated with either 12.5 μM of ESAT-6:CFP-10 or ESAT-6ΔC:CFP-10. After 2 h of protein treatment, cells were incubated with 6 μM of FITC labeled-holotransferrin in DMEM containing 2% BSA for 2 h. The control group received medium alone. Cells were fixed and visualized under confocal microscope (**A**). Fluorescence intensity of intracellular holotransferrin was quantified and shown as mean ± SEM of 50 cells of three independent experiments (**B**). Mice peritoneal macrophages were incubated with ^{55}Fe-transferrin and treated with either ESAT-6:CFP-10 or ESAT-6ΔC:CFP-10 protein. After 4 h of treatment, cells were lysed, and amount of radiolabeled iron incorporated into the cells was counted using liquid scintillation counter (**C**). Results were shown as mean ± SEM of three independent experiments.

of lack of processing in late Golgi, translocation of HFE to the cell surface is affected (45, 49, 50). Interestingly, in the current study, we demonstrated that ESAT-6:β2M interaction leads to accumulation of HFE in ER. Therefore, it can be concluded that *M. tuberculosis* targets the ESAT-6 protein to enrich HFE inside ER resulting in poorer surface HFE expression and inhibition of HFE:TFR1 complex formation. This can favor *M. tuberculosis* to alter iron homeostasis in the macrophage.

HFE is a key molecule that regulates iron homeostasis along with TFR1 at the surface of macrophage (33). HFE:TFR1 complex at the cell surface inhibits holotransferrin-mediated iron uptake (35). It is noticed that ESAT-6 enhanced holotransferrin-mediated iron uptake in macrophages. Interestingly, macrophage, when infected with H37Rv-WT strain, showed increased holotransferrin-mediated iron uptake as compared with H37Rv–ESAT-6–KO *M. tuberculosis* strain, indicating a direct role of ESAT-6 protein in accumulation of holotransferrin-meditated iron inside macrophages during *M. tuberculosis* infection. Iron is crucial for the growth of *M. tuberculosis* and important for its survival and pathogenesis (17, 51, 52). *M. tuberculosis* in phagosome acquires iron through transferrin pathway; *M. tuberculosis* secretes chelating agents like mycobactin that extract iron from the holotransferrin in the cytoplasm (2, 3). *M. tuberculosis* accumulates more iron in phagosome as compared with nonpathogenic strain like *M. smegmatis* (18). This further indicates that *M. tuberculosis* probably uses pathogenic factors like ESAT-6

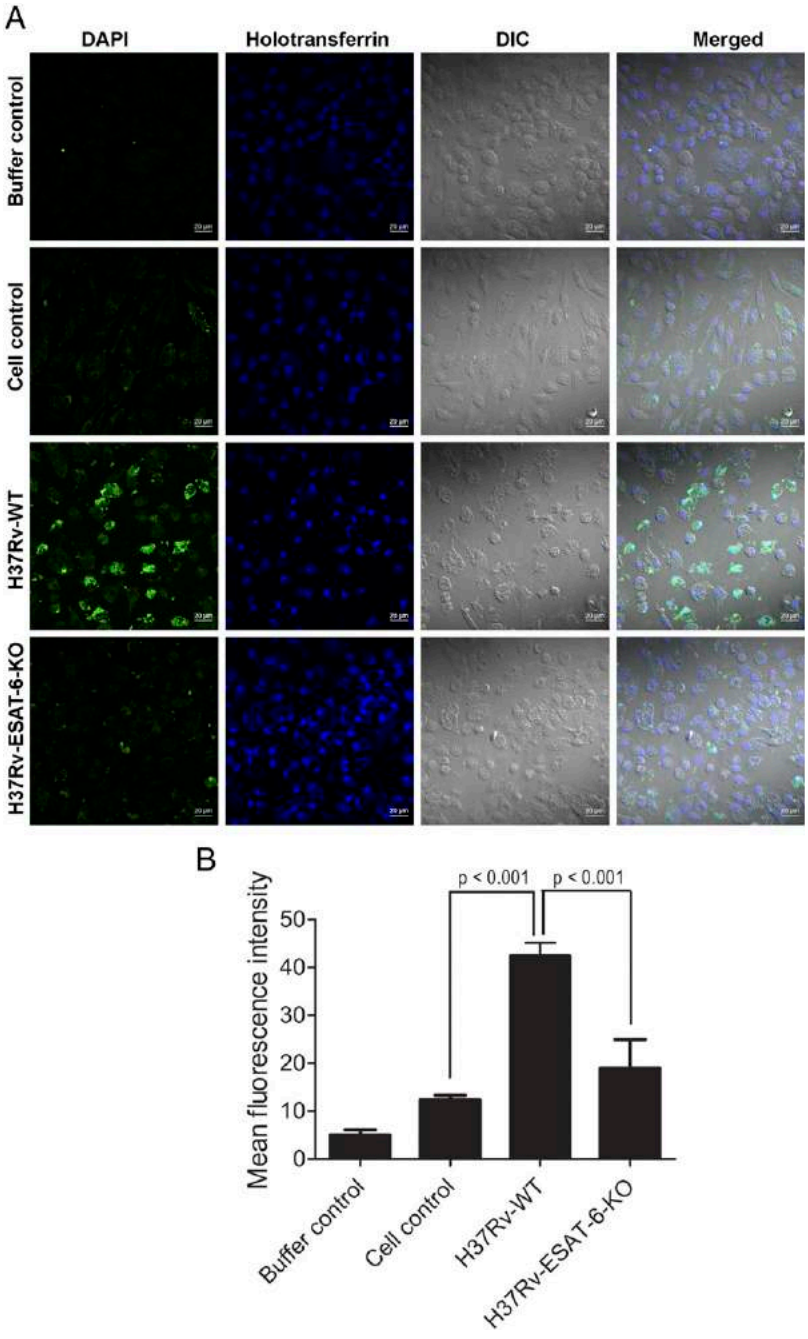

FIGURE 6. ESAT-6 elevates holotransferrin-mediated uptake of iron inside macrophage during *M. tuberculosis* infection. Peritoneal macrophages from C57BL/6 mice were infected with either H37Rv-WT or H37Rv–ESAT-6–KO *M. tuberculosis* strain at MOI of 1:10. Next, cells were incubated with 6 μM of FITC-labeled holotransferrin in incomplete DMEM containing 2% BSA. The cell control group received medium alone. After 2 h, cells were fixed and visualized under fluorescence microscope (**A**). Mean fluorescence intensity of intracellular holotransferrin was quantified and shown as mean ± SEM from 50 cells of three independent experiments (**B**).

to acquire host iron in the phagosome. A similar mechanism was identified in case of HIV-nef viral protein that down-regulates surface expression of HFE and modulates iron homeostasis in macrophages (53). Another viral protein HCMV-US2 is engaged in degradation of HFE and affects intracellular and surface expression of HFE, hence affects cellular metabolic functions regulated by iron (54). A recent study by Boradia et al. (4) reveals that *M. tuberculosis*–GAPDH binds to human holotransferrin, internalizes it, and transports across cell wall of mycobacterial cells. All these observations precisely indicate a role of HFE in regulating iron homeostasis. The present study highlights a novel tactic of *M. tuberculosis* using the ESAT-6 protein for regulation of iron that may help its better persistence. Thus, designing of small molecule inhibitors that can block ESAT-6:β2M interaction may be useful to improve protective immune responses of the host against mycobacterial infection.

Acknowledgments

We thank Dr. Lakshyaveer Singh, International Centre for Genetic Engineering and Biotechnology for the technical support for mycobacterial infection–related experiments. We also thank Dr. Komal Dolasia, CDFD, and Dr. Vartika Sharma, International Centre for Genetic Engineering and Biotechnology, for the help and intellectual discussion.

Disclosures

The authors have no financial conflicts of interest.

References

1. Cole, S. T., R. Brosch, J. Parkhill, T. Garnier, C. Churcher, D. Harris, S. V. Gordon, K. Eiglmeier, S. Gas, C. E. Barry, III, et al. 1998. Deciphering the biology of *Mycobacterium tuberculosis* from the complete genome sequence. *Nature* 393: 537–544.
2. Clemens, D. L., and M. A. Horwitz. 1996. The *Mycobacterium tuberculosis* phagosome interacts with early endosomes and is accessible to exogenously administered transferrin. *J. Exp. Med.* 184: 1349–1355.

3. Olakanmi, O., L. S. Schlesinger, A. Ahmed, and B. E. Britigan. 2002. Intraphagosomal *Mycobacterium tuberculosis* acquires iron from both extracellular transferrin and intracellular iron pools. Impact of interferon-gamma and hemochromatosis. *J. Biol. Chem.* 277: 49727–49734.
4. Boradia, V. M., H. Malhotra, J. S. Thakkar, V. A. Tillu, B. Vuppala, P. Patil, N. Sheokand, P. Sharma, A. S. Chauhan, M. Raje, and C. I. Raje. 2014. *Mycobacterium tuberculosis* acquires iron by cell-surface sequestration and internalization of human holo-transferrin. *Nat. Commun.* 5: 4730–4743.
5. Guinn, K. M., M. J. Hickey, S. K. Mathur, K. L. Zakel, J. E. Grotzke, D. M. Lewinsohn, S. Smith, and D. R. Sherman. 2004. Individual RD1-region genes are required for export of ESAT-6/CFP-10 and for virulence of *Mycobacterium tuberculosis*. *Mol. Microbiol.* 51: 359–370.
6. Renshaw, P. S., P. Panagiotidou, A. Whelan, S. V. Gordon, R. G. Hewinson, R. A. Williamson, and M. D. Carr. 2002. Conclusive evidence that the major T-cell antigens of the *Mycobacterium tuberculosis* complex ESAT-6 and CFP-10 form a tight, 1:1 complex and characterization of the structural properties of ESAT-6, CFP-10, and the ESAT-6*CFP-10 complex. Implications for pathogenesis and virulence. *J. Biol. Chem.* 277: 21598–21603.
7. Hsu, T., S. M. Hingley-Wilson, B. Chen, M. Chen, A. Z. Dai, P. M. Morin, C. B. Marks, J. Padiyar, C. Goulding, M. Gingery, et al. 2003. The primary mechanism of attenuation of *bacillus* Calmette-Guerin is a loss of secreted lytic function required for invasion of lung interstitial tissue. *Proc. Natl. Acad. Sci. USA* 100: 12420–12425.
8. de Jonge, M. I., G. Pehau-Arnaudet, M. M. Fretz, F. Romain, D. Bottai, P. Brodin, N. Honoré, G. Marchal, W. Jiskoot, P. England, et al. 2007. ESAT-6 from *Mycobacterium tuberculosis* dissociates from its putative chaperone CFP-10 under acidic conditions and exhibits membrane-lysing activity. *J. Bacteriol.* 189: 6028–6034.
9. Simeone, R., A. Bobard, J. Lippmann, W. Bitter, L. Majlessi, R. Brosch, and J. Enninga. 2012. Phagosomal rupture by *Mycobacterium tuberculosis* results in toxicity and host cell death. *PLoS Pathog.* 8: e1002507.
10. Sreejit, G., A. Ahmed, N. Parveen, V. Jha, V. L. Valluri, S. Ghosh, and S. Mukhopadhyay. 2014. The ESAT-6 protein of *Mycobacterium tuberculosis* interacts with beta-2-microglobulin (β2M) affecting antigen presentation function of macrophage. *PLoS Pathog.* 10: e1004446.
11. Bjorkman, P. J., M. A. Saper, B. Samraoui, W. S. Bennett, J. L. Strominger, and D. C. Wiley. 1987. Structure of the human class I histocompatibility antigen, HLA-A2. *Nature* 329: 506–512.
12. Feder, J. N., A. Gnirke, W. Thomas, Z. Tsuchihashi, D. A. Ruddy, A. Basava, F. Dormishian, R. Domingo, Jr., M. C. Ellis, A. Fullan, et al. 1996. A novel MHC class I-like gene is mutated in patients with hereditary haemochromatosis. *Nat. Genet.* 13: 399–408.
13. Martin, L. H., F. Calabi, F. A. Lefebvre, C. A. Bilsland, and C. Milstein. 1987. Structure and expression of the human thymocyte antigens CD1a, CD1b, and CD1c. *Proc. Natl. Acad. Sci. USA* 84: 9189–9193.
14. Gross, C. N., A. Irrinki, J. N. Feder, and C. A. Enns. 1998. Co-trafficking of HFE, a nonclassical major histocompatibility complex class I protein, with the transferrin receptor implies a role in intracellular iron regulation. *J. Biol. Chem.* 273: 22068–22074.
15. de Sousa, M., R. Reimão, R. Lacerda, P. Hugo, S. H. Kaufmann, and G. Porto. 1994. Iron overload in beta 2-microglobulin-deficient mice. *Immunol. Lett.* 39: 105–111.
16. Gomes-Pereira, S., P. N. Rodrigues, R. Appelberg, and M. S. Gomes. 2008. Increased susceptibility to *Mycobacterium avium* in hemochromatosis protein HFE-deficient mice. *Infect. Immun.* 76: 4713–4719.
17. Schaible, U. E., H. L. Collins, F. Priem, and S. H. Kaufmann. 2002. Correction of the iron overload defect in β-2-microglobulin knockout mice by lactoferrin abolishes their increased susceptibility to tuberculosis. *J. Exp. Med.* 196: 1507–1513.
18. Wagner, D., J. Maser, B. Lai, Z. Cai, C. E. Barry, III, K. Höner Zu Bentrup, D. G. Russell, and L. E. Bermudez. 2005. Elemental analysis of *Mycobacterium avium*-, *Mycobacterium tuberculosis*-, and *Mycobacterium smegmatis*-containing phagosomes indicates pathogen-induced microenvironments within the host cell's endosomal system. *J. Immunol.* 174: 1491–1500.
19. Banerjee, S., A. Farhana, N. Z. Ehtesham, and S. E. Hasnain. 2011. Iron acquisition, assimilation and regulation in mycobacteria. *Infect. Genet. Evol.* 11: 825–838.
20. Ratledge, C. 2004. Iron, mycobacteria and tuberculosis. *Tuberculosis (Edinb.)* 84: 110–130.
21. De Voss, J. J., K. Rutter, B. G. Schroeder, and C. E. Barry, III. 1999. Iron acquisition and metabolism by mycobacteria. *J. Bacteriol.* 181: 4443–4451.
22. Ahmed, A., K. Dolasia, and S. Mukhopadhyay. 2018. *Mycobacterium tuberculosis* PPE18 protein reduces inflammation and increases survival in animal model of sepsis. *J. Immunol.* 200: 3587–3598.
23. Zhang, X., R. Goncalves, and D. M. Mosser. 2008. The isolation and characterization of murine macrophages. *Curr. Protoc. Immunol.* 83: 14.1.1–14.1.14.
24. Bhat, K. H., A. Ahmed, S. Kumar, P. Sharma, and S. Mukhopadhyay. 2012. Role of PPE18 protein in intracellular survival and pathogenicity of *Mycobacterium tuberculosis* in mice. *PLoS One* 7: e52601.
25. Wahl, L. M., S. M. Wahl, L. E. Smythies, and P. D. Smith. 2006. Isolation of human monocyte populations. *Curr. Protoc. Immunol.* 70: 7.6A.1–7.6A.10.
26. Nair, S., P. A. Ramaswamy, S. Ghosh, D. C. Joshi, N. Pathak, I. Siddiqui, P. Sharma, S. E. Hasnain, S. C. Mande, and S. Mukhopadhyay. 2009. The PPE18 of *Mycobacterium tuberculosis* interacts with TLR2 and activates IL-10 induction in macrophage. *J. Immunol.* 183: 6269–6281.
27. Grenier, D., and S.-I. Tanabe. 2011. Transferrin as a source of iron for *Campylobacter rectus*. *J. Oral Microbiol.* DOI: 10.3402/jom.v3i0.5660.
28. Xiu-Lian, D., W. Kui, K. Ya, Y. Lan, L. Rong-Chang, C. Yan Zhong, H. Kwok Ping, and Q. Zhong Ming. 2004. Apotransferrin is internalized and distributed in the same way as holotransferrin in K562 cells. *J. Cell. Physiol.* 201: 45–54.
29. Waheed, A., J. H. Grubb, X. Y. Zhou, S. Tomatsu, R. E. Fleming, M. E. Costaldi, R. S. Britton, B. R. Bacon, and W. S. Sly. 2002. Regulation of transferrin-mediated iron uptake by HFE, the protein defective in hereditary hemochromatosis. *Proc. Natl. Acad. Sci. USA* 99: 3117–3122.
30. Srivastava, S., M. B. Battu, M. Z. Khan, V. K. Nandicoori, and S. Mukhopadhyay. 2019. *Mycobacterium tuberculosis* PPE2 protein interacts with $p67^{phox}$ and inhibits reactive oxygen species production. *J. Immunol.* 203: 1218–1229.
31. Renshaw, P. S., K. L. Lightbody, V. Veverka, F. W. Muskett, G. Kelly, T. A. Frenkiel, S. V. Gordon, R. G. Hewinson, B. Burke, J. Norman, et al. 2005. Structure and function of the complex formed by the tuberculosis virulence factors CFP-10 and ESAT-6. *EMBO J.* 24: 2491–2498.
32. Bennett, M. J., J. A. Lebrón, and P. J. Bjorkman. 2000. Crystal structure of the hereditary haemochromatosis protein HFE complexed with transferrin receptor. *Nature* 403: 46–53.
33. Feder, J. N., D. M. Penny, A. Irrinki, V. K. Lee, J. A. Lebrón, N. Watson, Z. Tsuchihashi, E. Sigal, P. J. Bjorkman, and R. C. Schatzman. 1998. The hemochromatosis gene product complexes with the transferrin receptor and lowers its affinity for ligand binding. *Proc. Natl. Acad. Sci. USA* 95: 1472–1477.
34. Lawrence, C. M., S. Ray, M. Babyonyshev, R. Galluser, D. W. Borhani, and S. C. Harrison. 1999. Crystal structure of the ectodomain of human transferrin receptor. *Science* 286: 779–782.
35. Salter-Cid, L., A. Brunmark, P. A. Peterson, and Y. Yang. 2000. The major histocompatibility complex-encoded class I-like HFE abrogates endocytosis of transferrin receptor by inducing receptor phosphorylation. *Genes Immun.* 1: 409–417.
36. Mwandumba, H. C., D. G. Russell, M. H. Nyirenda, J. Anderson, S. A. White, M. E. Molyneux, and S. B. Squire. 2004. *Mycobacterium tuberculosis* resides in nonacidified vacuoles in endocytically competent alveolar macrophages from patients with tuberculosis and HIV infection. *J. Immunol.* 172: 4592–4598.
37. Schnappinger, D., S. Ehrt, M. I. Voskuil, Y. Liu, J. A. Mangan, I. M. Monahan, G. Dolganov, B. Efron, P. D. Butcher, C. Nathan, and G. K. Schoolnik. 2003. Transcriptional adaptation of *Mycobacterium tuberculosis* within macrophages: insights into the phagosomal environment. *J. Exp. Med.* 198: 693–704.
38. Lounis, N., C. Truffot-Pernot, J. Grosset, V. R. Gordeuk, and J. R. Boelaert. 2001. Iron and *Mycobacterium tuberculosis* infection. *J. Clin. Virol.* 20: 123–126.
39. Pathak, S. K., S. Basu, K. K. Basu, A. Banerjee, S. Pathak, A. Bhattacharyya, T. Kaisho, M. Kundu, and J. Basu. 2007. Direct extracellular interaction between the early secreted antigen ESAT-6 of *Mycobacterium tuberculosis* and TLR2 inhibits TLR signaling in macrophages. [Published erratum appears in 2015 *Nat. Immunol.* 16: 326.] *Nat. Immunol.* 8: 610–618.
40. Sharma, B., R. Upadhyay, B. Dua, N. A. Khan, V. M. Katoch, B. Bajaj, and B. Joshi. 2015. *Mycobacterium tuberculosis* secretory proteins downregulate T cell activation by interfering with proximal and downstream T cell signalling events. *BMC Immunol.* 16: 67.
41. Ganguly, N., P. H. Giang, C. Gupta, S. K. Basu, I. Siddiqui, D. M. Salunke, and P. Sharma. 2008. Mycobacterium tuberculosis secretory proteins CFP-10, ESAT-6 and the CFP10:ESAT6 complex inhibit lipopolysaccharide-induced NF-kappaB transactivation by downregulation of reactive oxidative species (ROS) production. *Immunol. Cell Biol.* 86: 98–106.
42. Wang, X., P. F. Barnes, K. M. Dobos-Elder, J. C. Townsend, Y. T. Chung, H. Shams, S. E. Weis, and B. Samten. 2009. ESAT-6 inhibits production of IFN-γ by *Mycobacterium tuberculosis*-responsive human T cells. *J. Immunol.* 182: 3668–3677.
43. Lewis, K. N., R. Liao, K. M. Guinn, M. J. Hickey, S. Smith, M. A. Behr, and D. R. Sherman. 2003. Deletion of RD1 from *Mycobacterium tuberculosis* mimics bacille Calmette-Guérin attenuation. *J. Infect. Dis.* 187: 117–123.
44. Welin, A., D. Eklund, O. Stendahl, and M. Lerm. 2011. Human macrophages infected with a high burden of ESAT-6-expressing *M. tuberculosis* undergo caspase-1- and cathepsin B-independent necrosis. *PLoS One* 6: e20302.
45. Feder, J. N., Z. Tsuchihashi, A. Irrinki, V. K. Lee, F. A. Mapa, E. Morikang, C. E. Prass, S. M. Starnes, R. K. Wolff, S. Parkkila, et al. 1997. The hemochromatosis founder mutation in HLA-H disrupts β2-microglobulin interaction and cell surface expression. *J. Biol. Chem.* 272: 14025–14028.
46. Ajioka, R. S., and J. P. Kushner. 2002. Hereditary hemochromatosis. *Semin. Hematol.* 39: 235–241.
47. Bothwell, T. H., and A. P. MacPhail. 1998. Hereditary hemochromatosis: etiologic, pathologic, and clinical aspects. *Semin. Hematol.* 35: 55–71.
48. Pietrangelo, A. 2004. Hereditary hemochromatosis--a new look at an old disease. *N. Engl. J. Med.* 350: 2383–2397.
49. Waheed, A., S. Parkkila, X. Y. Zhou, S. Tomatsu, Z. Tsuchihashi, J. N. Feder, R. C. Schatzman, R. S. Britton, B. R. Bacon, and W. S. Sly. 1997. Hereditary hemochromatosis: effects of C282Y and H63D mutations on association with β2-microglobulin, intracellular processing, and cell surface expression of the HFE protein in COS-7 cells. *Proc. Natl. Acad. Sci. USA* 94: 12384–12389.
50. Zhou, X. Y., S. Tomatsu, R. E. Fleming, S. Parkkila, A. Waheed, J. Jiang, Y. Fei, E. M. Brunt, D. A. Ruddy, C. E. Prass, et al. 1998. HFE gene knockout produces mouse model of hereditary hemochromatosis. *Proc. Natl. Acad. Sci. USA* 95: 2492–2497.
51. Raghu, B., G. R. Sarma, and P. Venkatesan. 1993. Effect of iron on the growth and siderophore production of mycobacteria. *Biochem. Mol. Biol. Int.* 31: 341–348.

52. Cronjé, L., N. Edmondson, K. D. Eisenach, and L. Bornman. 2005. Iron and iron chelating agents modulate *Mycobacterium tuberculosis* growth and monocyte-macrophage viability and effector functions. *FEMS Immunol. Med. Microbiol.* 45: 103–112.
53. Drakesmith, H., N. Chen, H. Ledermann, G. Screaton, A. Townsend, and X. N. Xu. 2005. HIV-1 Nef down-regulates the hemochromatosis protein HFE, manipulating cellular iron homeostasis. *Proc. Natl. Acad. Sci. USA* 102: 11017–11022.
54. Vahdati-Ben Arieh, S., N. Laham, C. Schechter, J. W. Yewdell, J. E. Coligan, and R. Ehrlich. 2003. A single viral protein HCMV US2 affects antigen presentation and intracellular iron homeostasis by degradation of classical HLA class I and HFE molecules. *Blood* 101: 2858–2864.